

Constraining primordial magnetic fields with distortions of the black-body spectrum of the cosmic microwave background: pre- and post-decoupling contributions

Kerstin E. Kunze,^a Eiichiro Komatsu^{b,c}

^aDepartamento de Física Fundamental and IUFFyM, Universidad de Salamanca, Plaza de la Merced s/n, 37008 Salamanca, Spain

^bMax-Planck-Institut für Astrophysik, Karl-Schwarzschild Str. 1, 85741 Garching, Germany

^cKavli Institute for the Physics and Mathematics of the Universe, Todai Institutes for Advanced Study, the University of Tokyo, Kashiwa, Japan 277-8583 (Kavli IPMU, WPI)

E-mail: kkunze@usal.es, komatsu@mpa-garching.mpg.de

Abstract. Primordial magnetic fields that exist before the photon-baryon decoupling epoch are damped on length scales below the photon diffusion and free-streaming scales. The energy injected into the plasma by dissipation of magnetosonic and Alfvén waves heats photons, creating a y -type distortion of the black-body spectrum of the cosmic microwave background. This y -type distortion is converted into a μ -type distortion when elastic Compton scattering is efficient. Therefore, we can use observational limits on y - and μ -type distortions to constrain properties of magnetic fields in the early universe. Assuming a Gaussian, random, and non-helical field, we calculate μ and y as a function of the present-day strength of the field, B_0 , smoothed over a certain Gaussian width, k_c^{-1} , as well as of the spectral index of the power spectrum of fields, n_B , defined by $P_B(k) \propto k^{n_B}$. For a nearly scale-invariant spectrum with $n_B = -2.9$ and a Gaussian smoothing width of $k_c^{-1} = 1$ Mpc, the existing COBE/FIRAS limit on μ yields $B_0 < 40$ nG, whereas the projected PIXIE limit on μ would yield $B_0 < 0.8$ nG. For non-scale-invariant spectra, constraints can be stronger. For example, for $B_0 = 1$ nG with $k_c^{-1} = 1$ Mpc, the COBE/FIRAS limit on μ excludes a wide range of spectral indices given by $n_B > -2.6$. After decoupling, energy dissipation is due to ambipolar diffusion and decaying MHD turbulence, creating a y -type distortion. The distortion is completely dominated by decaying MHD turbulence, and is of order $y \approx 10^{-7}$ for a few nG field smoothed over the damping scale at the decoupling epoch, $k_{d,dec} \approx 290 (B_0/1 \text{ nG})^{-1} \text{ Mpc}^{-1}$. This contribution is as large as those of the known contributions such as reionization at a redshift of $z \approx 10$ and virialized objects at lower redshifts. The projected PIXIE limit on y would exclude $B_0 > 1.0$ and 0.6 nG for $n_B = -2.9$ and -2.3 , respectively, and $B_0 > 0.6$ nG for $n_B \geq 2$. Finally, we find that the current limits on the optical depth to Thomson scattering restrict the predicted y -type distortion to be $y \lesssim 10^{-8}$.

Contents

1	Introduction	1
2	Pre-decoupling era	2
2.1	Damping of primordial magnetic fields	2
2.2	Energy injection rate	3
2.3	CMB distortions	5
2.4	Results	6
2.4.1	μ -type distortion	6
2.4.2	y -type distortion	8
3	Post-decoupling era	9
3.1	Ambipolar diffusion	9
3.2	Decaying MHD turbulence	12
3.3	Results	13
3.3.1	Evolution of electron temperature and ionization fraction	13
3.3.2	y -type distortion	15
3.4	Optical depth to Thomson scattering	17
4	Conclusions	19
5	Acknowledgements	20
A	Photon diffusion scale	20

1 Introduction

The cosmic microwave background (CMB) is a nearly perfect black body [1–3]. The thermal spectrum observed today is the result of its continuous evolution during the history of the universe. In the early universe, $z \gtrsim 2 \times 10^6$, a black-body spectrum is established by bremsstrahlung [4, 5] and double-Compton scattering [6, 7]. Subsequent injections of energy into the plasma in $z \lesssim 2 \times 10^6$ may distort the black-body spectrum [8–10].

When energy is injected into the plasma after $z \approx 2 \times 10^6$, heated electrons alter the photon spectrum via elastic Compton scattering. Unlike bremsstrahlung and double-Compton scattering, elastic Compton scattering does not alter the number of photons, and thus the equilibrium distribution of photons after energy injection is a Bose-Einstein distribution with a non-vanishing chemical potential, μ . The photon occupation number distribution is then given by $n(x) = (e^{x+\mu} - 1)^{-1}$, where $x \equiv h\nu/(k_B T)$ is a dimensionless frequency of photons. If elastic scattering is not efficient enough for the equilibrium distribution to be reached, the distribution of photons takes on a y -type distortion [9, 10] or an intermediate form between μ - and y -type distortions [11, 12], depending on the nature and epoch of energy injection.

Acoustic waves in the photon-baryon plasma before the photon-baryon decoupling epoch are damped on length scales below the photon diffusion scale (which is often called the “Silk damping scale”) [13–15]. This damping injects energy into the plasma, creating a y -type distortion [16–18]. This process can also be understood as a superposition of black-body

spectra with different temperatures [19, 20]. Recent calculations show that only 1/3 of the injected energy creates a y -type distortion, while the remaining 2/3 of the energy raises the temperature of photons [20–22].

If magnetic fields exist before the decoupling epoch, they are similarly damped [23, 24], creating μ - and y -type distortions [25]. After the decoupling epoch, magnetic fields are damped by different mechanisms (ambipolar diffusion and decaying magnetohydrodynamical (MHD) turbulence [26]), again creating a y -type distortion. In this paper, we first reexamine the calculation of μ - and y -type distortions due to damping of magnetic fields in the pre-decoupling era (section 2). We then present the calculation of a y -type distortion as well as of the optical depth to Thomson scattering due to damping of magnetic fields in the *post*-decoupling era (section 3). Finally, we conclude in section 4. We use the best-fit cosmological parameters from the WMAP 9-year data only [27] for the numerical calculations presented in this paper.

2 Pre-decoupling era

2.1 Damping of primordial magnetic fields

While there is one acoustic (compressible) mode in a non-magnetized plasma in the early universe, there are three modes in a magnetized plasma. Two are compressible and are called “fast” and “slow” magnetosonic waves, while the other is incompressible and is called an “Alfvén” wave [23, 24]. Magnetosonic waves perturb the plasma density as well as the magnetic field, and are scalar modes in linear perturbation theory. An Alfvén wave perturbs the field but does not perturb the density, and is a vector mode in linear perturbation theory.

The evolution of these modes is rather complex, depends on the ratios of damping and driving terms, and is in general quite different from damping of acoustic waves in a non-magnetized photon-baryon plasma. Nevertheless, the analyses given in Refs. [23, 24] provide a rather simple picture. For weak fields, the (time-dependent) oscillation frequency of the fast mode is given by $\omega = \pm v_s(k/a)$, where k is the comoving wavenumber; $v_s = 1/\sqrt{3(1+R)}$ is the sound speed of the photon-baryon plasma; $R \equiv 3\rho_b/(4\rho_\gamma) \propto a$; a is the Robertson-Walker scale factor; and ρ_b and ρ_γ are energy densities of baryons and photons, respectively. (We take the speed of light to be unity.) The fast mode damps in the same way as the acoustic wave in a non-magnetized plasma, and thus its damping wavenumber, k_d , is determined by the inverse of the usual photon diffusion scale, k_γ ; namely, the fast mode is damped by an exponential factor of $\exp(-k^2/k_d^2)$ with $k_d = k_\gamma$, where [15]

$$\frac{1}{k_\gamma^2} \equiv \frac{1}{6} \int \frac{dt}{a^2(1+R)} l_\gamma \left(\frac{16}{15} + \frac{R^2}{1+R} \right). \quad (2.1)$$

Here, $l_\gamma \equiv 1/(\sigma_T n_e)$ is the mean free path of photons. In a deeply radiation-dominated era in which $R \ll 1$, we have $k_\gamma^{-2} \rightarrow (8/45) \int dt l_\gamma/a^2$.

The oscillation frequencies of the slow and Alfvén modes are equal to $\omega = \pm V_A \cos \theta(k/a)$ (up to the leading order in the field value), where θ is an angle between the wave vector and the field direction, and $V_A = \tilde{B}/\sqrt{1+R}$ is the Alfvén velocity with

$$\tilde{B} \equiv \frac{B}{\sqrt{16\pi\rho_\gamma/3}} \simeq 3.8 \times 10^{-4} \left(\frac{B_0}{1 \text{ nG}} \right). \quad (2.2)$$

Here, $B_0 a_0^2 \equiv B a^2$ is the present-day field value assuming magnetic flux freezing. These modes also damp in a similar way as the fast mode, if their comoving wavelength is longer

than $l_\gamma/(aV_A \cos \theta)$. However, in the opposite limit in which their comoving wavelength is shorter than $l_\gamma/(aV_A \cos \theta)$, these modes become *over-damped* and are nearly frozen. They survive damping until their comoving wavelength becomes comparable to $l_\gamma/a \ll l_\gamma/(aV_A)$. In this free-streaming regime, the slow and Alfvén modes with the comoving wavelength shorter than $v_A \cos \theta$ times the photon diffusion scale are damped, i.e., $k_d = k_\gamma/(v_A \cos \theta)$, where

$$v_A \equiv \tilde{B} = V_A \sqrt{1 + R}, \quad (2.3)$$

is the Alfvén velocity calculated during the radiation-dominated era (in which $R \ll 1$).

The longest comoving damping wavelength (i.e., smallest k_d) is given by that at the decoupling epoch, $z = z_{\text{dec}} = 1088$. Modeling the recombination history following Ref. [28] and using the exact expression of the photon diffusion scale given in eq. (2.1), we find

$$k_{d,\text{dec}} = \frac{286.91}{\cos \theta} \left(\frac{B_0}{1 \text{ nG}} \right)^{-1} \text{ Mpc}^{-1}, \quad (2.4)$$

for the best-fit Λ CDM model from the WMAP 9-year data only (see Appendix A for details). The wavenumbers of the slow and Alfvén modes contributing to the observed μ - and y -type distortions are *larger* than this value.¹

2.2 Energy injection rate

We calculate the energy injection rate, \dot{Q} , as a rate at which the field energy density changes due to damping of magnetosonic and Alfvén waves: $\dot{Q} = -a^{-4}d(\rho_B a^4)/dt$.

Let us define the comoving magnetic energy density, $\rho_{B,0}$, as

$$\rho_{B,0}(\vec{x})a_0^4 \equiv \rho_B(\vec{x}, t)a^4, \quad (2.5)$$

where the subscript 0 indicates the present time. In our units, $\rho_{B,0}(\vec{x}) = \frac{1}{2}\tilde{B}_0^2(\vec{x})$, where $B_0 a_0^2 \equiv B a^2$.

We assume that a field is a non-helical and Gaussian random field with the two-point correlation function in Fourier space given by

$$\langle B_i^*(\vec{k}) B_j(\vec{q}) \rangle = (2\pi)^3 \delta(\vec{k} - \vec{q}) P_B(k) \left(\delta_{ij} - \frac{k_i k_j}{k^2} \right), \quad (2.6)$$

where the power spectrum, $P_B(k)$, is assumed to be a power law, $P_B(k) = A_B k^{n_B}$, with the amplitude, A_B , and the spectral index, n_B .

As the energy density of fields, $\rho_{B,0}$, is proportional to B_0^2 , the ensemble average of $\rho_{B,0}$ is given by the power spectrum as

$$\langle \rho_{B,0} \rangle = \int \frac{d^3 k}{(2\pi)^3} P_{B,0}(k) e^{-2\left(\frac{k}{k_c}\right)^2}, \quad (2.7)$$

¹Note that only the photon diffusion scale (the Silk damping scale) is important for distortions of the CMB spectrum. In the evolution of a primordial magnetic field, neutrino decoupling marks another important epoch for damping of a field. Similarly to photon free-streaming, neutrino free-streaming damps magnetosonic and Alfvén waves, injecting energy into the plasma. The corresponding damping scale is given in Ref. [24]. However, neutrino decoupling takes place at $z \sim 10^{10}$, at which time the elastic as well as double-Compton scattering is very effective, and a black-body spectrum is restored. Therefore, an energy injection due to dissipation of a field by neutrino free-streaming does not cause any observable distortion of the CMB spectrum.

where k_c is a certain Gaussian smoothing scale. Using $\rho_{B,0}$ instead of $A_{B,0}$, we write the present-day power spectrum as

$$P_{B,0}(k) = \frac{4\pi^2}{k_c^3} \frac{2^{(n_B+3)/2}}{\Gamma\left(\frac{n_B+3}{2}\right)} \left(\frac{k}{k_c}\right)^{n_B} \langle \rho_{B,0} \rangle. \quad (2.8)$$

The ‘‘scale-invariant’’ case corresponds to $n_B \rightarrow -3$, in which the contribution to the energy density per logarithmic wavenumber, $d\ln\langle\rho_{B,0}\rangle/d\ln k \propto k^3 P_{B,0}(k) e^{-2(k/k_c)^2}$, is independent of wavenumbers (up to smoothing). Spectral indices of fields generated during inflation are usually negative [29], whereas they are positive for fields generated by causal processes such as the electroweak phase transition [30–36]. Moreover, in the latter case n_B has to be an even integer and $n_B \geq 2$ [37].

For the calculation of the energy injection rate, $\dot{Q} = -a^{-4}d(\rho_B a^4)/dt$, we take the smoothing scale to be the damping scale, k_d , and obtain

$$\begin{aligned} a^4 \langle \rho_B \rangle(z) &= a^4 \int \frac{d^3k}{(2\pi)^3} P_B(k) e^{-2\left(\frac{k}{k_d(z)}\right)^2} \\ &= a_0^4 \int \frac{d^3k}{(2\pi)^3} P_{B,0}(k) e^{-2\left(\frac{k}{k_d(z)}\right)^2}. \end{aligned} \quad (2.9)$$

The energy injection rate is thus found to be

$$\frac{dQ}{dz} = \frac{n_B + 3}{2} \left(\frac{\rho_{B,0}}{\rho_{\gamma,0}} \right) k_c^{-(n_B+3)} k_d(z)^{n_B+5} \frac{d}{dz} k_d^{-2}(z), \quad (2.10)$$

where we have used $\Gamma[(n_B+5)/2] = [(n_B+3)/2]\Gamma[(n_B+3)/2]$, and ρ_γ and $\rho_{\gamma,0}$ are the photon energy densities at a given time and the present time, respectively. We have removed $\langle \rangle$ from $\rho_{B,0}$ for a simpler notation.

Let us write the damping scale as $k_d = \alpha k_\gamma$, where $\alpha = 1$ for the fast magnetosonic mode and $\alpha = v_A^{-1} \simeq 2.6 \times 10^3$ (1 nG/ B_0) for the slow and Alfvén modes.² For $n_B \geq -3$, the energy injection rate by dissipation of the slow and Alfvén modes is greater than that of the fast mode. As we consider only $n_B \geq -3$ in this paper, we shall use $\alpha = v_A^{-1}$ for the rest of this paper. Finally, we shall assume energy equipartition of the fast, slow, and Alfvén modes, which will introduce an additional factor of 2/3 to eq. (2.10). Note that this is a non-trivial assumption: if, for some reason, the slow and Alfvén modes are highly suppressed relative to the fast mode, our analysis does not apply.

Deep inside the radiation-dominated era, $z \gg z_{eq} = 3265$ [27], the photon diffusion scale is well approximated by $k_\gamma^{-2} = A_\gamma^2 z^{-3}$ with $A_\gamma^2 = 5.9807 \times 10^{10}$ Mpc² for the best-fit parameters from the WMAP 9-year data only (see Appendix A for details). The energy injection rate thus becomes (after multiplying eq. (2.10) by 2/3 for equipartition)

$$\frac{dQ}{dz} = -(n_B + 3) \left(\frac{\rho_{B,0}}{\rho_{\gamma,0}} \right) \left(\frac{\alpha A_\gamma^{-1/2}}{k_c} \right)^{n_B+3} (1+z)^{\frac{3n_B+7}{2}}. \quad (2.11)$$

For $n_B < -7/3$, the energy injection rate decreases with redshifts; thus, the largest contribution comes from the lowest redshift under consideration. For $n_B > -7/3$, the largest contribution comes from the highest redshift under consideration, i.e., $z \approx 2 \times 10^6$, above which the distribution becomes a Planck distribution.

²In principle, we should perform the integration over angles in eq. (2.9) taking into account the fact that the damping scale for the slow and Alfvén modes depends on angles as $k_d = k_\gamma/(v_A \cos\theta)$. We shall ignore this subtlety and take $\cos\theta = 1$. This simplification provides a lower limit to the energy injection rate.

2.3 CMB distortions

There are three main processes determining the final CMB spectrum: elastic Compton scattering, double Compton scattering, and bremsstrahlung. Ref. [6] finds that double Compton scattering dominates over bremsstrahlung in the relevant epoch.

At $z \gtrsim 2 \times 10^6$, double Compton scattering is efficient and photons have a Planck distribution. At $z \lesssim 2 \times 10^6$, double Compton scattering is no longer efficient enough to erase signatures of energy injection. However, as long as elastic Compton scattering is efficient, the distribution approaches a Bose-Einstein distribution with a non-vanishing μ . This is the so-called “ μ -era,” which occurs between redshifts of $5 \times 10^4 \lesssim z \lesssim 2 \times 10^6$ [38]. (Strictly speaking, the distortion takes on an intermediate form between μ - and y -type distortions in $1.5 \times 10^4 \lesssim z \lesssim 2 \times 10^5$ [11, 12], but we shall ignore this subtlety.) During the subsequent “ y -era,” elastic Compton scattering is no longer efficient and the photon spectrum cannot relax to a Bose-Einstein distribution; thus, the distortion remains a y -type.

The time evolution of μ is determined by [39]

$$\frac{d\mu}{dt} = -\frac{\mu}{t_{DC}(z)} + \frac{1.4}{3} \frac{dQ}{\rho_\gamma dt}, \quad (2.12)$$

where a factor of 1/3 in the second term accounts for a recent finding that only 1/3 of the energy injection contributes to spectral distortions [20–22].³ Here, t_{DC} is the time scale for double Compton scattering,

$$t_{DC} = 2.06 \times 10^{33} \left(1 - \frac{Y_P}{2}\right)^{-1} (\Omega_b h^2)^{-1} z^{-\frac{9}{2}} \text{ s}, \quad (2.13)$$

where $Y_P = 0.24$ is the primordial helium mass abundance. The solution of this equation during the radiation era is

$$\mu = \frac{1.4}{3} \int_{z_1}^{z_2} dz \frac{dQ}{\rho_\gamma dz} e^{-\left(\frac{z}{z_{DC}}\right)^{\frac{5}{2}}}, \quad (2.14)$$

where the integration is done for the μ -era, i.e., $z_1 = 2 \times 10^6$ and $z_2 = 5 \times 10^4$, and

$$z_{DC} \equiv 1.97 \times 10^6 \left[1 - \frac{1}{2} \left(\frac{Y_P}{0.24}\right)\right]^{-\frac{5}{2}} \left(\frac{\Omega_b h^2}{0.0224}\right)^{-\frac{2}{5}}. \quad (2.15)$$

Since the μ -era is well within the radiation-dominated era, the energy injection rate is given by eq. (2.11). Thus,

$$\begin{aligned} \mu = & -\frac{1.4}{3} (n_B + 3) \left(\frac{\rho_{B,0}}{\rho_{\gamma,0}}\right) \left[\frac{1.08 \times 10^{-2} \left(\frac{B_0}{\text{nG}}\right)^{-1}}{k_c / \text{Mpc}^{-1}}\right]^{n_B+3} \\ & \times \int_{z_1}^{z_2} dz (1+z)^{\frac{3n_B+7}{2}} e^{-\left(\frac{z}{z_{DC}}\right)^{\frac{5}{2}}}, \end{aligned} \quad (2.16)$$

³The same factor of 1/3 applies to energy injection by dissipation of magnetosonic and Alfvén waves. The magnetic field is coupled to electrons. Upon dissipation it heats electrons, raising the electron temperature, T_e . Photons and electrons are tightly coupled so that $T_\gamma = T_e$, i.e., any change in the electron temperature is transmitted to the photon temperature. Therefore, energy injection due to dissipation of the magnetosonic and Alfvén waves is similar to that of the acoustic waves in a non-magnetized photon-baryon fluid: injection of the magnetic field energy leads to a mixture of black body spectra for which it has been shown that 1/3 of the injected energy leads to spectral distortions and 2/3 to raise the average temperature.

with $\frac{\rho_{B,0}}{\rho_{\gamma,0}} = 9.545 \times 10^{-8} \left(\frac{B_0}{\text{nG}}\right)^2$ for $T_{\text{cmb}} = 2.725$ K [40].

For $z < z_2$, elastic Compton scattering is no longer effective, and thus the distortion remains a y -type. The Compton y -parameter is given by [21]

$$y = \frac{1}{12} \int_{z_2}^{z_{\text{dec}}} dz \frac{dQ}{\rho_{\gamma}}, \quad (2.17)$$

where $z_{\text{dec}} = 1088$ is the decoupling epoch [27]. In this era the universe is matter-dominated, and we use the full expression for the photon diffusion scale with the recombination history given by Ref. [28]. We shall discuss the post-decoupling contributions separately in section 3.

2.4 Results

There are three free parameters: the present-day field value, B_0 , smoothed over a certain Gaussian width of k_c^{-1} , and the spectral index, n_B . Among these, n_B and k_c should be determined by a mechanism by which fields are generated.⁴

For fields generated during inflation, k_c can take on any values, while n_B required to produce strong enough fields on cosmological scales is usually negative. The correlation length of fields generated by causal processes such as a phase transition should be determined by the horizon size of the relevant phase transition (QCD or electroweak), while n_B is positive and causality requires n_B to be even integers with $n_B \geq 2$ [37].

For numerical calculations we use $Y_P = 0.24$ and $\Omega_b h^2 = 0.02264$ [27, 40].

2.4.1 μ -type distortion

First, we set k_c^{-1} to be the maximal damping wavelength at decoupling (eq. (2.4) with $\cos \theta = 1$). Figure 1 (left) shows the predicted values of μ as a function of B_0 and n_B . The left and right panels show n_B expected from inflation and phase transitions, respectively.

We find that the COBE/FIRAS limit, $|\mu| < 9 \times 10^{-5}$ [3] (blue dotted lines), yields $B_0 < 40$ nG for a nearly scale-invariant spectrum, $n_B = -2.9$. The projected PIXIE limit, $|\mu| < 5 \times 10^{-8}$ [41] (red dot-dashed lines), would yield an order of magnitude stronger constraint, $B_0 < 0.9$ nG, for $n_B = -2.9$. For non-scale-invariant spectra, $n_B > -2.9$, the constraints are much stronger. For example, the COBE/FIRAS limit and the projected PIXIE limit yield $B_0 < 0.4$ and 10^{-2} nG, respectively, for $n_B = -2.2$. For $n_B \geq 2$ expected from phase transitions, the largest B_0 allowed by the COBE/FIRAS limit is of the order of 10^{-11} nG, which can be improved to 3×10^{-13} nG using PIXIE.

The left panel of figure 2 shows how sensitive the inferred values of B_0 are to the assumed values of k_c for $n_B = 2$. For example, the projected PIXIE limit is satisfied for, say, $B_0 = 1$ nG, as long as $k_c > 3 \times 10^7$ Mpc⁻¹, or a present-day smoothing width of < 0.2 pc. Figure 3 shows the same for $n_B = -2.9$ (left panel) and -2.4 (right panel).

The right panel of figure 2 is more interesting. It shows which pairs of (B_0, n_B) are allowed for a given value of $k_c = 1$ Mpc⁻¹. We find $B_0 < 10^{-4}$ nG for $n_B > -2.0$ from the COBE/FIRAS limit. On the other hand, for $B_0 = 1$ nG, the COBE/FIRAS limit excludes $n_B > -2.6$. Both limits can be improved significantly by PIXIE.

⁴Alternatively, one may simply take k_c to be a convenient normalization scale at which limits on B_0 are reported.

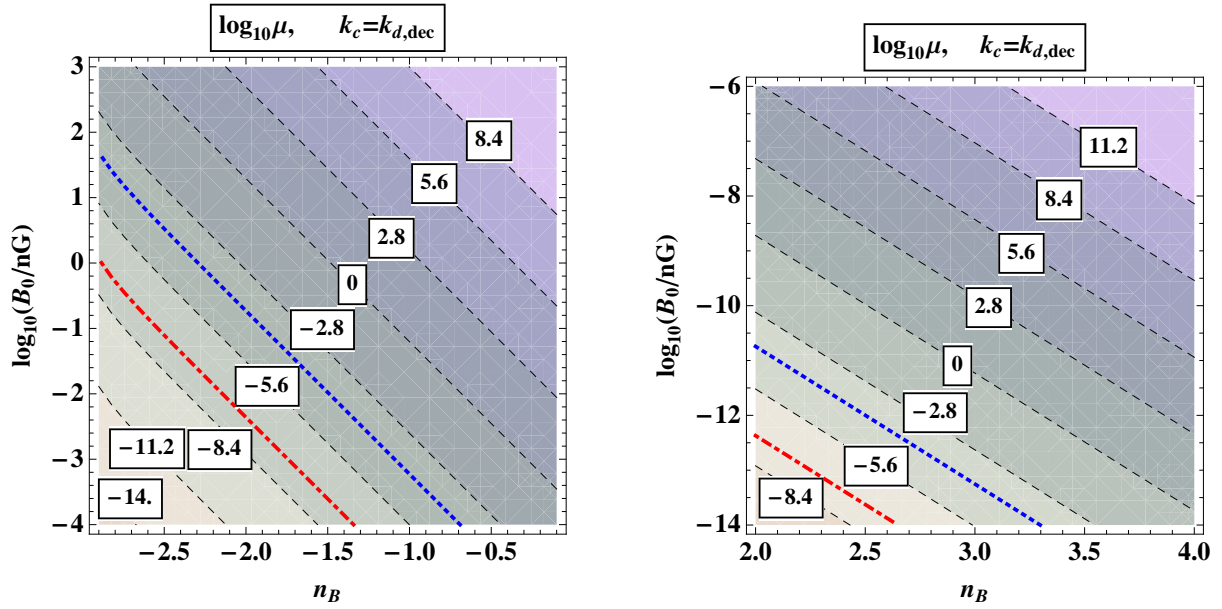


Figure 1. Contour plots of $\log_{10} \mu$ in the (B_0, n_B) plane for n_B expected from inflation (left panel) and phase transitions (right panel). The smoothing scale is set to be the maximal value of the damping wavelength at decoupling (eq. (2.4) with $\cos \theta = 1$). The blue (dotted) lines show the COBE/FIRAS limit, $\mu = 9.0 \times 10^{-5}$ [3], and the red (dot-dashed) lines show the projected PIXIE limit, $\mu = 5.0 \times 10^{-8}$ [41].

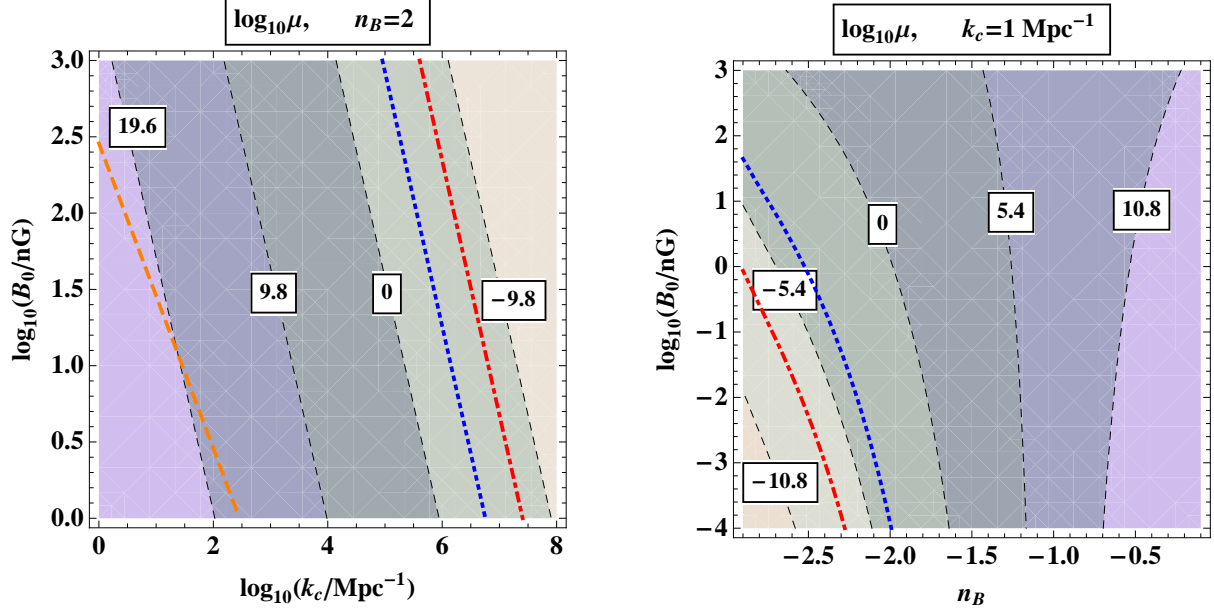


Figure 2. Contour plots of $\log_{10} \mu$ in the (B_0, k_c) plane for a fixed index $n_B = 2$ (left panel) and in the (B_0, n_B) plane for a fixed smoothing scale $k_c = 1 \text{ Mpc}^{-1}$ (right panel). The blue (dotted) lines show the COBE/FIRAS limit, $\mu = 9.0 \times 10^{-5}$ [3], and the red (dot-dashed) lines show the projected PIXIE limit, $\mu = 5.0 \times 10^{-8}$ [41]. The orange (dashed) line in the left panel shows k_c corresponding to the maximal value of the damping wavelength at decoupling (eq. (2.4) with $\cos \theta = 1$).

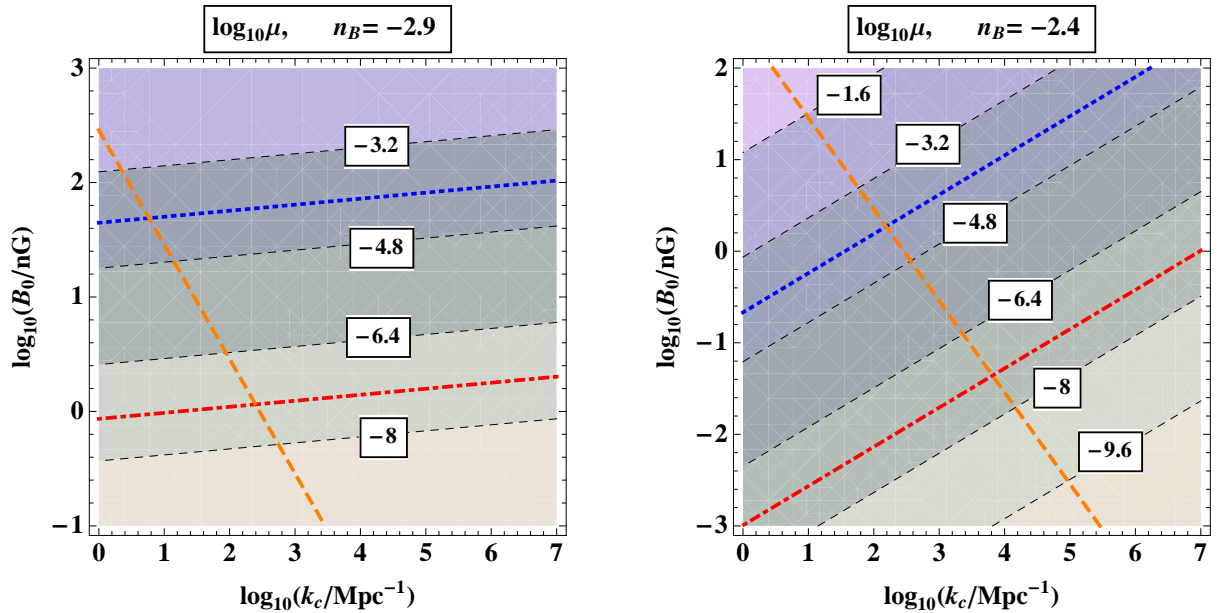


Figure 3. Same as the left panel of figure 2, but for $n_B = -2.9$ (left panel) and -2.4 (right panel).

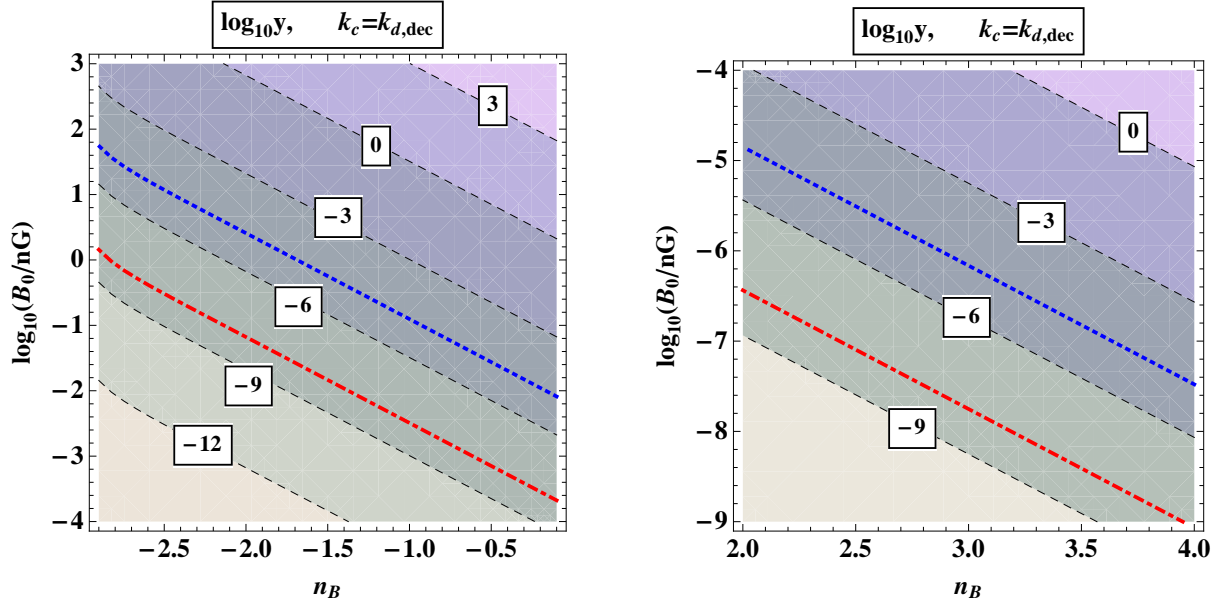


Figure 4. Same as figure 1 but for $\log_{10} y$.

2.4.2 y -type distortion

Next, we calculate the y -type distortion due to dissipation of slow magnetosonic and Alfvén waves using eq. (2.17). Comparing figures 4 and 1 (also see figure 6), and the left panel of figure 5 and the right panel of figure 2 (also see figure 7), we find that constraints on the parameters of primordial magnetic fields from the y -type distortion is much weaker than those from the μ -type distortion for non-scale-invariant spectra, $n_B > -3$. The reason is simple: as the y -type distortion is created by energy injection at lower redshifts, $z \lesssim 5 \times 10^4$,

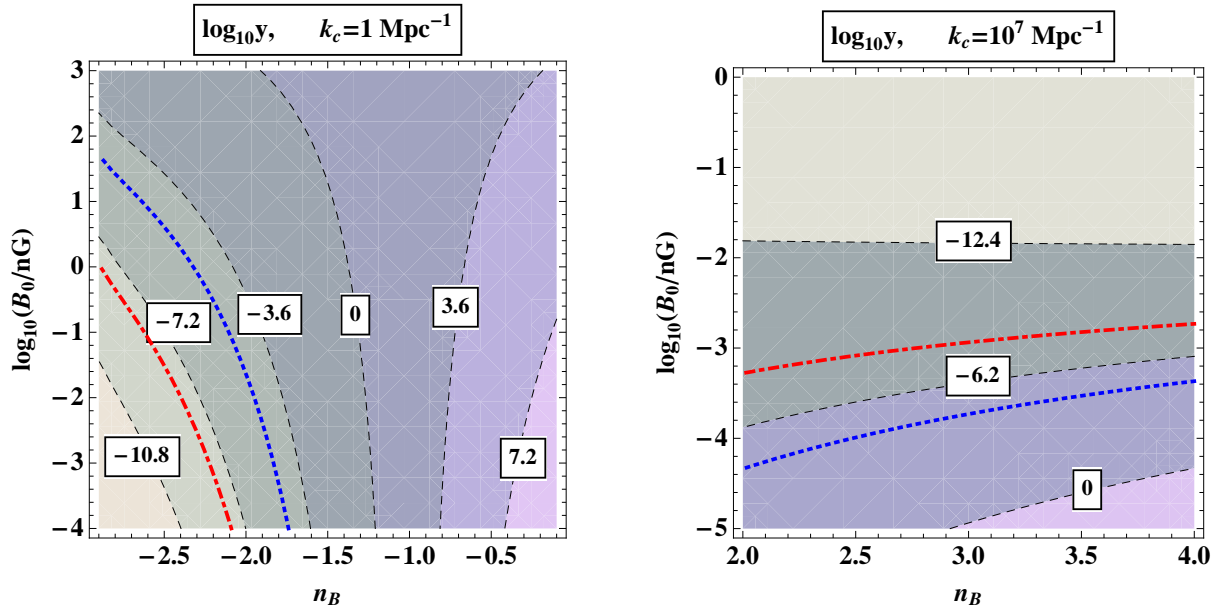


Figure 5. Same as the right panel of figure 2, but for $\log_{10} y$ (left panel) and for $\log_{10} y$, $k_c = 10^7 \text{ Mpc}^{-1}$, and $2 \leq n_B \leq 4$ (right panel).

the damping wavenumber for the y -type distortion is much smaller than that for the μ -type distortion. As a result, the dissipated magnetic energy creating the y -type distortion is much smaller than that for the μ -distortion for non-scale-invariant spectra, $n_B > -3$. For a scale-invariant spectrum, such a change in the damping wavenumber does not affect the result much, and thus y - and μ -type distortions are equally powerful for constraining the parameters of primordial magnetic fields.

3 Post-decoupling era

After the decoupling epoch, there are two processes by which the magnetic field can dissipate energy into the intergalactic medium. Firstly, there is ambipolar diffusion which arises due to the existence of a remnant ionized component in the nearly completely neutral plasma after decoupling. Secondly, non-linear effects can lead to decaying MHD turbulence. In this section, we shall follow Sethi and Subramanian [26] to compute heating of the intergalactic medium (IGM) due to dissipation of fields via ambipolar diffusion and decaying MHD turbulence, and then compute the y -type distortion from inverse Compton scattering of CMB photons off those heated electrons in the IGM.

3.1 Ambipolar diffusion

Ambipolar diffusion has its origin in the velocity difference between the neutral and ionized components of matter due to the Lorentz force only acting on the ionized component. The ionized components that are accelerated by the Lorentz force share their kinetic energy with the neutral components via ion-neutral collisions, heating the IGM. Therefore, the energy in magnetic fields is dissipated into the IGM, as the velocity difference between ionized and neutral components is damped by the collisions.

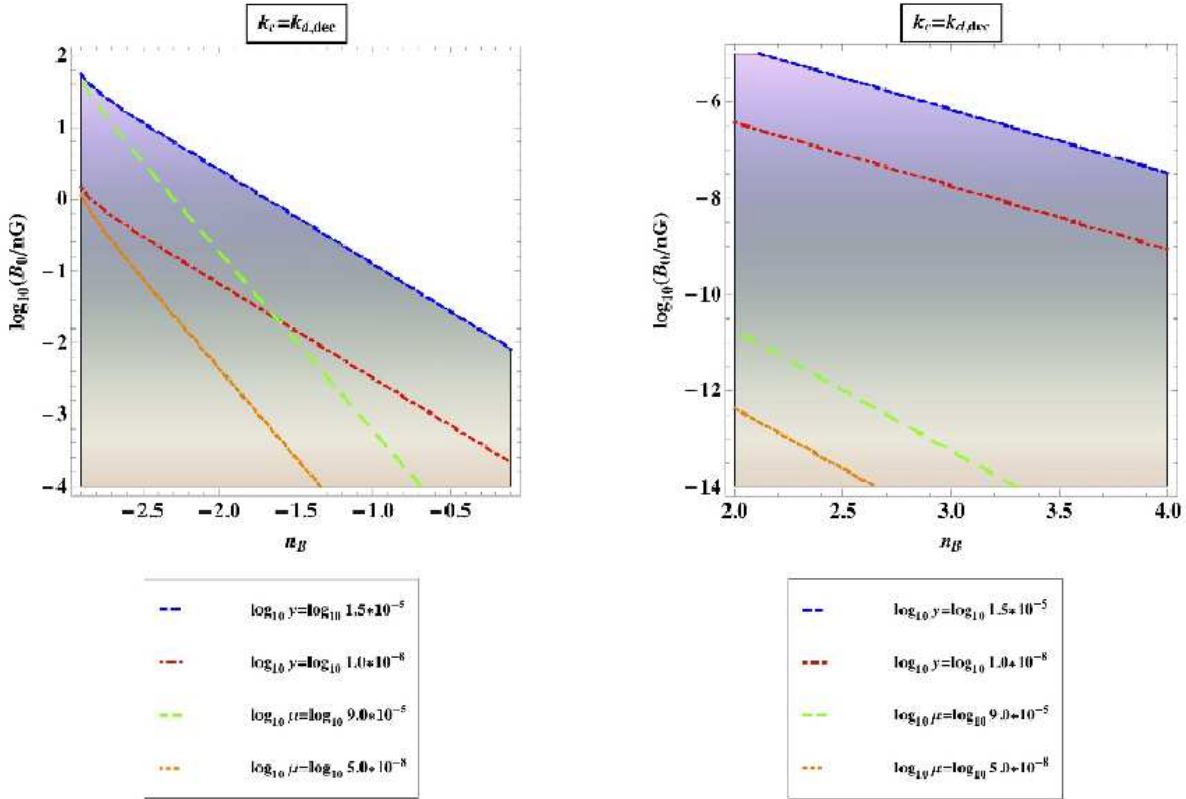


Figure 6. Comparison of constraints on B_0 and n_B from pre-decoupling μ - and y -type distortions. The left and right panels show n_B expected from inflation and phase transitions, respectively. The smoothing scale is set to be the maximal value of the damping wavelength at decoupling (eq. (2.4) with $\cos\theta = 1$). The blue (short-dashed) and green (long-dashed) lines show the COBE/FIRAS limits, $y = 1.5 \times 10^{-5}$ and $\mu = 9.0 \times 10^{-5}$ [3], respectively. The red (dot-dashed) and orange (dotted) lines show the projected PIXIE limits, $y = 10^{-8}$ and $\mu = 5.0 \times 10^{-8}$ [41], respectively.

The volume rate of energy dissipation due to ambipolar diffusion is proportional to the average Lorentz force squared, and is given by [26]

$$\Gamma_{\text{in}} = \frac{\rho_n}{16\pi^2\gamma\rho_b^2\rho_i} |(\vec{\nabla} \times \vec{B}) \times \vec{B}|^2, \quad (3.1)$$

where ρ_n , ρ_i , and ρ_b are the energy densities of neutral hydrogen, ionized hydrogen, and the total baryons, respectively, and γ is the coupling between the ionized and neutral component given by $\gamma \simeq \langle\sigma v\rangle_{H^+,H}/(2m_H)$, where $\langle\sigma v\rangle_{H^+,H} = 0.649 T^{0.375} \times 10^{-9} \text{ cm}^3 \text{ s}^{-1}$ [42].

In the Lorentz force, $\vec{L} = (\vec{\nabla} \times \vec{B}) \times \vec{B}$, the derivative operator is defined with respect to the proper coordinates. The flux freezing thus gives a strong redshift evolution of the Lorentz force, $\vec{L} \propto (1+z)^5$. Recalling $\rho_n/\rho_i \propto (1-x_e)/x_e$ and $\rho_b \propto (1+z)^3$, we find that the energy dissipation rate via ambipolar diffusion evolves as $\Gamma_{\text{in}} \propto (1+z)^{3.625}(1-x_e)/x_e$ when the matter temperature goes as $T \propto 1/a$, and $\propto (1+z)^{3.25}(1-x_e)/x_e$ when $T \propto 1/a^2$. On the other hand, as we shall show later, the energy dissipation rate via decaying MHD turbulence evolves as $\Gamma_{\text{decay}} \propto (1+z)^{11/2}$ (see eq. (3.6)); thus, the ambipolar diffusion dominates at lower redshifts.

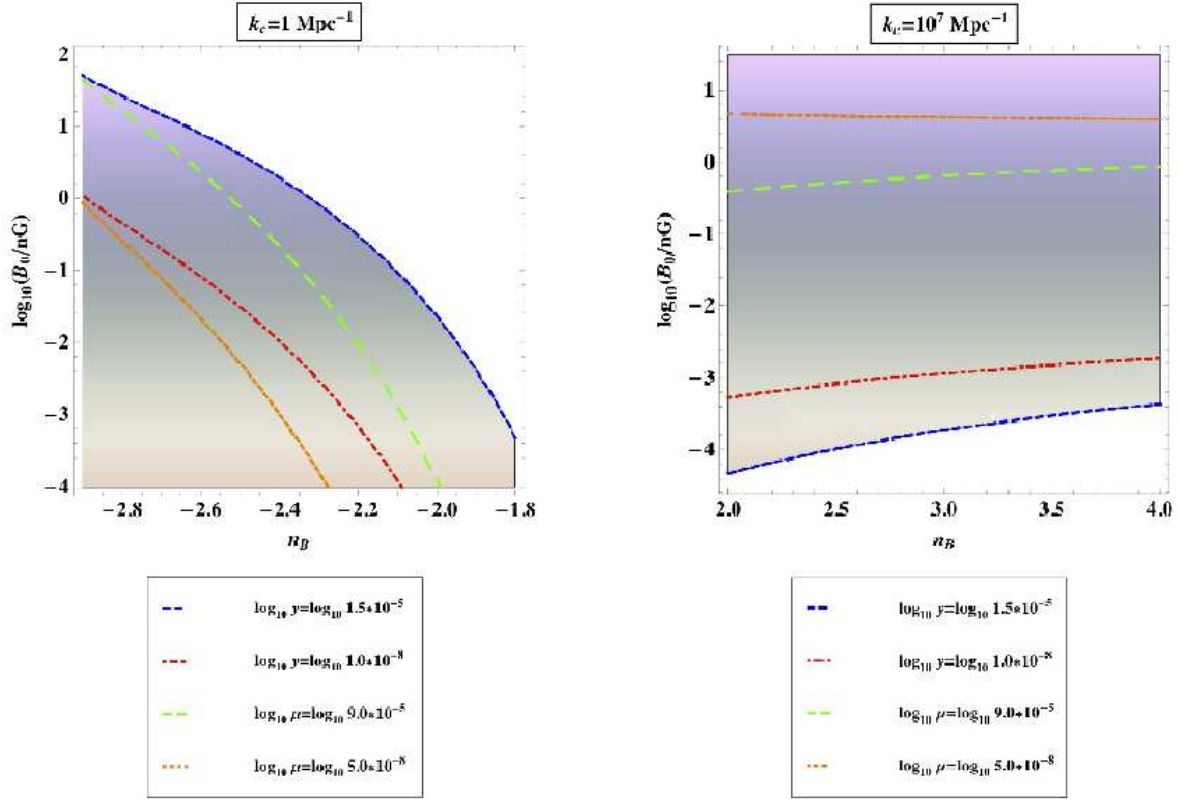


Figure 7. Comparison of constraints on B_0 and n_B from pre-decoupling μ - and y -type distortions. (Left panel) Same as the left panel of figure 6, but for $k_c = 1 \text{ Mpc}^{-1}$ and $-2.9 \leq n_B \leq -1.8$. (Right panel) Same as the right panel of figure 6, but for $k_c = 10^7 \text{ Mpc}^{-1}$.

If velocities can still be treated as linear perturbations, the baryon velocity in the standard Λ CDM model is a scalar mode. Therefore, the velocity differences between the ionized and neutral components are determined by the corresponding scalar mode of the Lorentz force (e.g., [43]):

$$L_i = \frac{\rho_\gamma}{3a} \sum_{\vec{k}} k L(\vec{k}) Y_i(\vec{k}, \vec{x}), \quad (3.2)$$

where $Y_i = -k^{-1} Y_{|i}$. In flat space, the scalar harmonics have the representation of $Y(\vec{k}, \vec{x}) = e^{i\vec{k}\cdot\vec{x}}$. The power spectrum of magnetic fields can be used to find the corresponding power spectrum of $L(\vec{k})$ defined by

$$\langle L^*(\vec{k}) L(\vec{q}) \rangle = (2\pi)^3 \delta(\vec{k} - \vec{q}) P_L(k). \quad (3.3)$$

In Ref. [43], $P_L(k)$ has been calculated using a Gaussian damping with a width of k_d^{-1} as in section 2. The average Lorentz force is then given by

$$\begin{aligned} \langle \vec{L}^2(\vec{r}, z) \rangle &= \frac{k_d^2 \rho_{B,0}^2}{[\Gamma(\frac{n_B+3}{2})]^2} (1+z)^{10} \int_0^\infty dw w^{2n_B+7} e^{-w^2} \int_0^\infty dv v^{n_B+2} e^{-2v^2 w^2} \int_{-1}^1 dx e^{2w^2 vx} \\ &\times (1 - 2vx + v^2)^{\frac{n_B-2}{2}} [1 + 2v^2 + (1 - 4v^2)x^2 - 4vx^3 + 4v^2 x^4], \end{aligned} \quad (3.4)$$

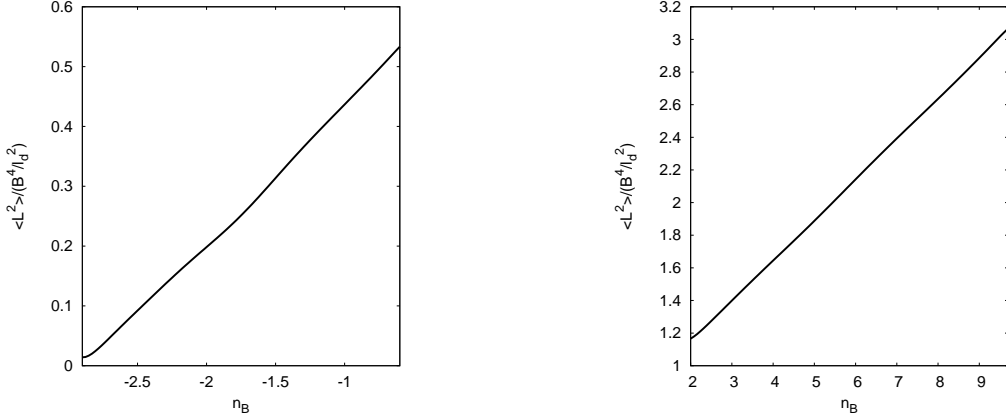


Figure 8. Ratio of the average Lorentz term calculated from eq. (3.5) and B^4/l_d^2 as a function of n_B .

where $w = k/k_d$, $v = q/k$, and $x = \frac{\vec{k} \cdot \vec{q}}{kq}$. This can be written in terms of $B(z)$ and $l_d = k_d^{-1}/(1+z)$, so that

$$\begin{aligned} \langle \vec{L}^2(\vec{r}, z) \rangle &= \left(\frac{B^4(z)}{l_d^2(z)} \right) \frac{1}{4 [\Gamma(\frac{n_B+3}{2})]^2} \int_0^\infty dw w^{2n_B+7} e^{-w^2} \int_0^\infty dv v^{n_B+2} e^{-2v^2w^2} \int_{-1}^1 dx e^{2w^2vx} \\ &\times (1 - 2vx + v^2)^{\frac{n_B-2}{2}} [1 + 2v^2 + (1 - 4v^2)x^2 - 4vx^3 + 4v^2x^4]. \end{aligned} \quad (3.5)$$

In Refs. [42, 44] the average Lorentz term has been approximated by B^4/l_d^2 . In figure 8, we show the ratio of the average Lorentz term calculated from eq. (3.5) and B^4/l_d^2 . Clearly B^4/l_d^2 is not a good approximation, and thus we shall use eq. (3.5) unless indicated otherwise. Moreover, k_d is chosen to be $k_{d,dec}$ given in eq. (2.4) with $\cos \theta = 1$.

3.2 Decaying MHD turbulence

Turbulent motion in the plasma is suppressed before the decoupling epoch due to a large radiative viscosity. However, it is no longer suppressed after the decoupling epoch, and the Reynolds number becomes very large. On scales smaller than the magnetic Jeans length, non-linear mode interactions transfer energy to smaller scales, dissipating the magnetic field on larger scales and inducing MHD turbulence to decay.

One can use results of numerical simulations of MHD turbulence in flat space to calculate the evolution of magnetic fields in an expanding universe, by rescaling variables [45, 46]. The estimated decay rate for a non-helical field in the matter-dominated era is given by [26]

$$\Gamma_{\text{decay}} = \frac{B_0^2}{8\pi} \frac{3m}{2} \frac{\left[\ln \left(1 + \frac{t_d}{t_i} \right) \right]^m}{\left[\ln \left(1 + \frac{t_d}{t_i} \right) + \ln \left[\left(\frac{1+z_i}{1+z} \right)^{\frac{3}{2}} \right] \right]^{m+1}} H(t) (1+z)^4, \quad (3.6)$$

where B_0 is again the present-day field value assuming a flux freezing; m is related to the magnetic spectral index as $m = \frac{2(n_B+3)}{n_B+5}$; t_d is the physical decay time scale for turbulence given by $t_d/t_i = (k_J/k_d)^{\frac{(n_B+5)}{2}} \simeq 14.8 (B_0/1 \text{ nG})^{-1} (k_d/1 \text{ Mpc}^{-1})^{-1}$ with the magnetic Jeans wavenumber of $k_J \simeq 14.8 \frac{2}{n_B+5} (B_0/1 \text{ nG})^{-\frac{2}{n_B+5}} (k_d/1 \text{ Mpc}^{-1})^{\frac{n_B+3}{n_B+5}} \text{ Mpc}^{-1}$ [26]; and z_i and

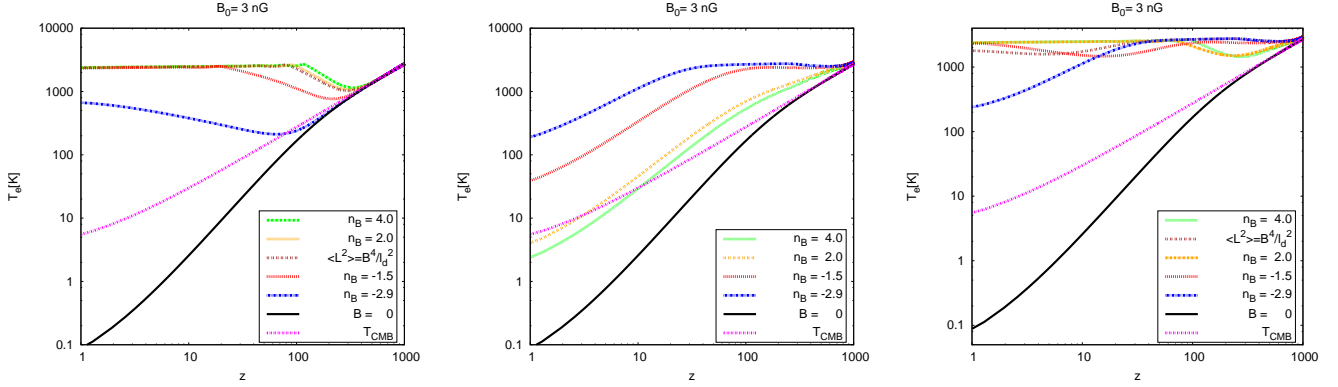


Figure 9. Evolution of the matter temperature with and without dissipation of magnetic fields. (Left panel) Dissipation by ambipolar diffusion. (Middle panel) Dissipation by decaying MHD turbulence. (Right panel) Both contributions are included. For all cases, a present-day magnetic field of $B_0 = 3$ nG, smoothed over $k_{d,dec}$ (eq. (2.4) with $\cos\theta = 1$), is assumed. We explore four different values of the spectral index ($n_B = -2.9, -1.5, 2$, and 4). The black solid lines (the bottom line in each panel) do not include dissipation of magnetic fields. The magenta dotted lines (the second to the bottom line in each panel) show the CMB temperature. The brown dotted lines in the left and right panels use the approximation for the squared Lorentz force, $\langle L^2 \rangle = B^4/l_d^2$; otherwise we use eq. (3.5).

t_i are the redshift and time at which dissipation of the magnetic field due to decaying MHD turbulence becomes important. We use $z_i = z_{dec} = 1088$ [27].

Ignoring a logarithmic dependence on $1 + z$, we find that the energy dissipation rate via decaying MHD turbulence evolves as $\Gamma_{decay} \propto (1 + z)^{11/2}$, which is faster than that of ambipolar diffusion (see eq. (3.1)). Therefore, we expect dissipation via decaying turbulence to dominate in early times.

3.3 Results

3.3.1 Evolution of electron temperature and ionization fraction

The evolution of the electron temperature is determined by [26]

$$\dot{T}_e = -2\frac{\dot{a}}{a}T_e + \frac{x_e}{1+x_e} \frac{8\rho_\gamma\sigma_T}{3m_e c} (T_\gamma - T_e) + \frac{x_e\Gamma}{1.5k_B n_e}, \quad (3.7)$$

where $\Gamma = \Gamma_{in}$ for ambipolar diffusion; $\Gamma = \Gamma_{decay}$ for energy dissipation due to decaying MHD turbulence; and $\Gamma = \Gamma_{in} + \Gamma_{decay}$ when both are included in the calculation.

The evolution of the ionization fraction, x_e , is not directly affected by magnetic fields, but it is indirectly affected by changes in T_e (i.e., higher T_e gives more collisional ionization in the IGM). The system of equations determining the thermal and ionization history of the universe has been solved in the absence of magnetic fields [47–56]. We have modified a public code **RECFAST++**⁵, which is the C version of **RECFAST**⁶ with some improvements, by including Γ_{in} and Γ_{decay} in the evolution equation of T_e .

Figure 9 shows the evolution of electron temperature with and without dissipation of magnetic fields. The left and middle panels include the contribution of either ambipolar

⁵http://www.cita.utoronto.ca/~jchluba/Science_Jens/Recombination/Recfast++.html

⁶<http://www.astro.ubc.ca/people/scott/recfast.html>

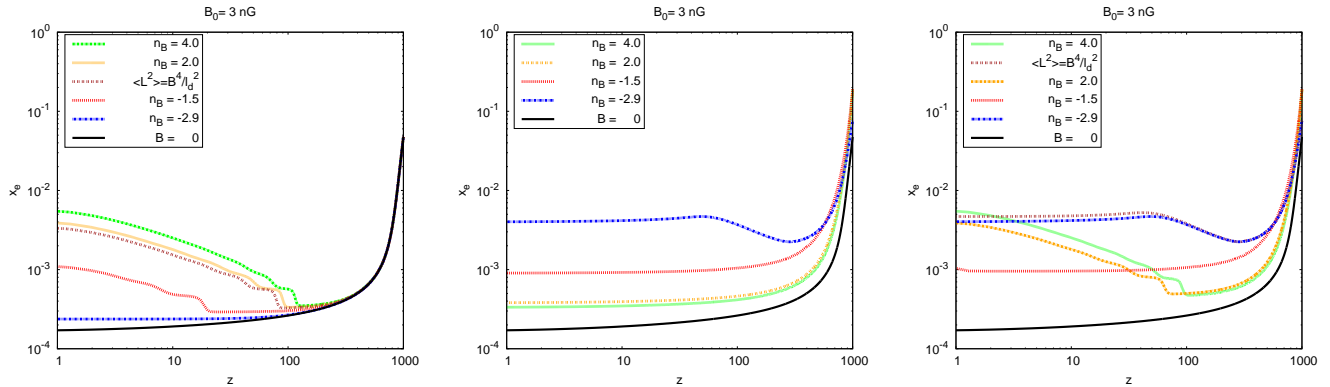


Figure 10. Evolution of the ionization fraction, x_e , with and without dissipation of magnetic fields. (Left panel) Dissipation by ambipolar diffusion. (Middle panel) Dissipation by decaying MHD turbulence. (Right panel) Both contributions are included. For all cases, a present-day magnetic field of $B_0 = 3$ nG, smoothed over $k_{d,dec}$ (eq. (2.4) with $\cos\theta = 1$), is assumed. We explore four different values of the spectral index ($n_B = -2.9, -1.5, 2$, and 4). The black solid lines (the bottom line in each panel) do not include dissipation of magnetic fields. The brown dotted lines in the left and right panels use the approximation for the squared Lorentz force, $\langle L^2 \rangle = B^4/l_d^2$; otherwise we use eq. (3.5).

diffusion or decaying MHD turbulence, respectively, and the right panel includes both contributions. Compared with non-magnetized case (the bottom black solid line in each panel), we find that dissipation of magnetic fields raises the electron temperature by many orders of magnitude. Ambipolar diffusion and decaying MHD turbulence heat the gas at different epochs: the former is important at $z \lesssim 100$ while the latter is important at $z \gtrsim 100$. This is consistent with our expectation based on how the energy dissipate rate evolves: $\Gamma_{in} \propto (1+z)^{3.625}(1-x_e)/x_e$ for $T \propto 1/a$ and $(1+z)^{3.25}(1-x_e)/x_e$ for $T \propto 1/a^2$, and $\Gamma_{decay} \propto (1+z)^{5.5}$.

When both contributions are included, we find that the temperature is raised at roughly all redshifts. For $B_0 = 3$ nG, we find that the temperature is raised up to about 2600 K, which is only a factor of about four lower than a typical temperature of photo-ionized gas (10^4 K).

We also find that the dependence of the temperature on n_B is opposite for ambipolar diffusion and decaying MHD turbulence. For ambipolar diffusion, the larger the spectral index n_B is, the higher the temperature becomes, while the opposite happens for decaying MHD turbulence. This is because of the scales at which dissipation occurs. For ambipolar diffusion, small-scale fields are dissipated. For decaying MHD turbulence, energy in large-scale fields is transferred to small scales and dissipates. Mathematically, Γ_{in} is proportional to the Lorentz force squared, which is proportional to B^4 with a factor of k^2 via spatial derivatives, whereas Γ_{decay} is proportional to the energy density of fields, B^2 .

Figure 10 shows the evolution of ionization fraction, x_e . For $B_0 = 3$ nG, the ionization fraction can reach of order 10^{-3} or more, which is an order of magnitude greater than x_e without dissipation of magnetic fields. The dependence of x_e on n_B is also similar to that of T_e . An important implication of this calculation for the ionization history of the universe is that there can be a significant, of order 0.1%, ionization even at $z \approx 100$. Dissipation of magnetic fields plays only a sub-dominant role at $z \lesssim 10$, in which the ionization fraction reaches unity by reionization of the universe by first stars.

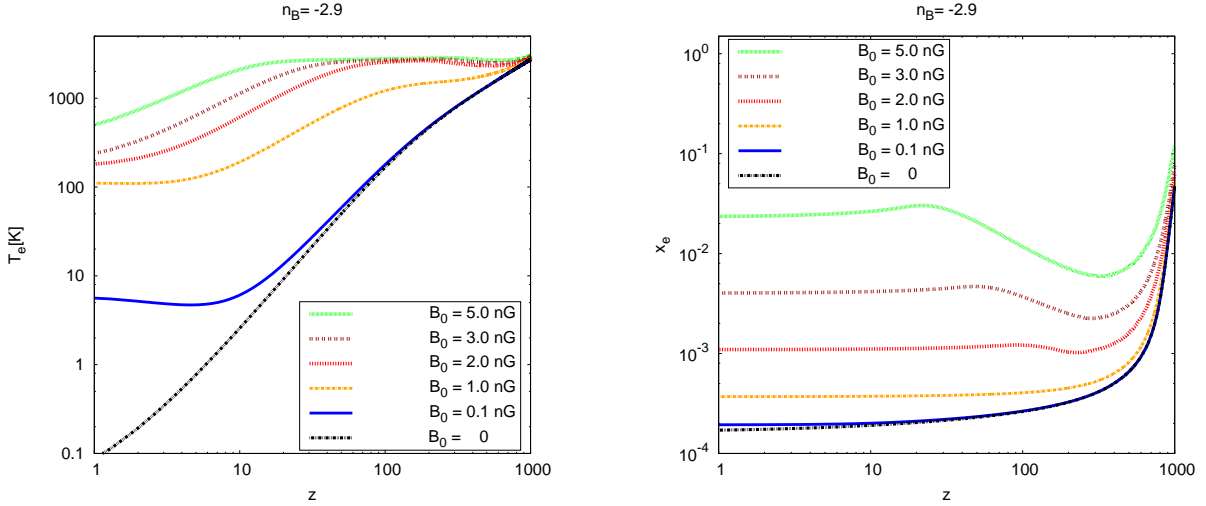


Figure 11. Evolution of the matter temperature (left panel) and the ionization fraction (right panel) with and without dissipation of magnetic fields. From top to bottom lines, the field values are $B_0 = 5, 3, 2, 1, 0.1,$ and 0 nG, and the magnetic power spectrum is nearly scale invariant with $n_B = -2.9$. Both ambipolar diffusion and decaying MHD turbulence are included.

The rate of energy dissipation due to ambipolar diffusion is proportional to B_0^4 (see eq. (3.1)) and that due to decaying MHD turbulence is proportional to B_0^2 (up to logarithmic dependence; see eq. (3.6)). Therefore, we would expect a strong dependence of T_e and x_e on B_0 . Figure 11 shows that T_e and x_e depend sensitively on B_0 ; however, T_e at $z \gtrsim 100$ does not increase by going from 2 nG to 5 nG. This is because the plasma cools efficiently by the inverse Compton scattering of the CMB photons off electrons at high redshifts, and thus the temperature cannot rise indefinitely.

3.3.2 y -type distortion

We calculate the y -type distortion using

$$y = - \int_{z_i}^{z_0} \frac{dz}{(1+z)} \frac{n_e \sigma_{TC} k_B (T_e - T_{CMB})}{H(z) m_e c^2}, \quad (3.8)$$

where $z_i = z_{\text{dec}} = 1088$ [27] and $z_0 = 10^{-4}$.

Figure 12 shows the predicted y values for $-2.9 \leq n_B \leq 0$ (left panel) and $2 \leq n_B \leq 9$ (right panel). There are two important results. First, the predicted values of y are quite sizable, $y \approx 10^{-7}$, for a few nG fields. These values are comparable to the contributions from virialized halos in $z \lesssim 5$ via the thermal Sunyaev-Zel'dovich effect, $y_{\text{tSZ}} \approx 1.7 \times 10^{-6}$ [57], and the reionization of the universe at $5 \lesssim z \lesssim 10$, $y_{\text{reion}} \approx 1.5 \times 10^{-7}$. (The latter contribution is given by $y \approx \tau k_B T_e / (m_e c^2) \approx 1.5 \times 10^{-7}$ for $\tau = 0.09$ [27] and $T_e = 10^4$ K = 0.862 eV.)

Second, the predicted values of y are insensitive to n_B for $n_B \gtrsim -2$ and depend only weakly on n_B for $-2.9 \leq n_B \lesssim -2$. This is because most of the y -type distortion is generated in early times, $z \gtrsim 100$, when the electron density is high (i.e., $n_e \propto x_e (1+z)^3$) and the contribution from decaying MHD turbulence completely dominates over that from ambipolar diffusion. For a given field strength B_0 , the energy injection from decaying MHD turbulence depends on n_B only via $m = 2(n_B + 3)/(n_B + 5)$ (see eq. (3.6)), which varies slowly with n_B unless n_B is close to -3 .

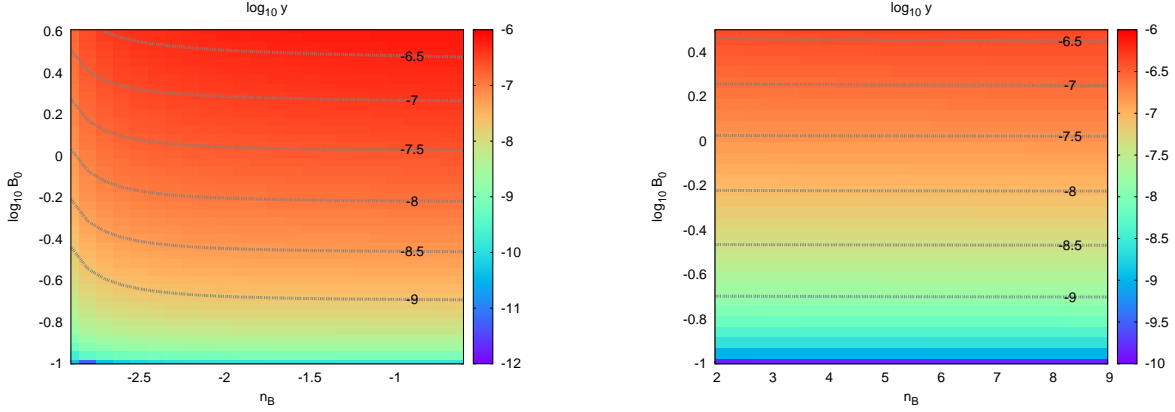


Figure 12. Predicted y -type distortion from dissipation of magnetic fields in the post-decoupling era due to ambipolar diffusion and decaying MHD turbulence as a function of the present-day field value, B_0 , smoothed over $k_{d,dec}$ (eq. (2.4) with $\cos\theta = 1$), and the spectral index, n_B . The left panel shows $-2.9 \leq n_B \leq 0$ while the right panel shows $2 \leq n_B \leq 9$.

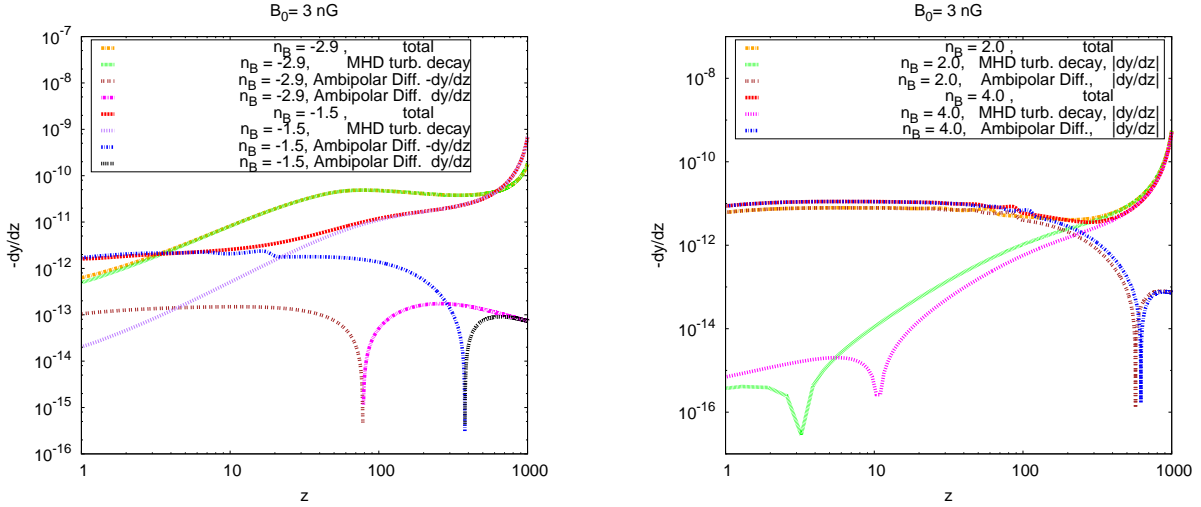


Figure 13. Contribution to the integrand in eq. (3.8), $-\frac{dy}{dz}$, from dissipation of magnetic fields in the post-decoupling era due to ambipolar diffusion and decaying MHD turbulence as a function of the present-day field value, B_0 , smoothed over $k_{d,dec}$ given in eq. (2.4) with $\cos\theta = 1$, and the spectral index, n_B . The left panel shows negative spectral indices while the right panel shows positive ones. For all cases, a present-day magnetic field of $B_0 = 3$ nG is assumed.

Figure 13 shows the contributions to the integrand of y in eq. (3.8), that is, $-\frac{dy}{dz}$, for $B_0 = 3$ nG. The y -type distortion is completely dominated by decaying MHD turbulence for $n_B = -2.9$ at all redshifts (see the left panel). As n_B increases, the ambipolar diffusion contribution dominates at lower redshifts (see the right panel). However, dissipation via decaying MHD turbulence continues to be the dominant contribution at $z \gtrsim 200$ even for $n_B = 4$. As the dominant contribution to the y -type distortion comes from high redshifts where the electron density is high, decaying MHD turbulence always dominates in y for all values of n_B .

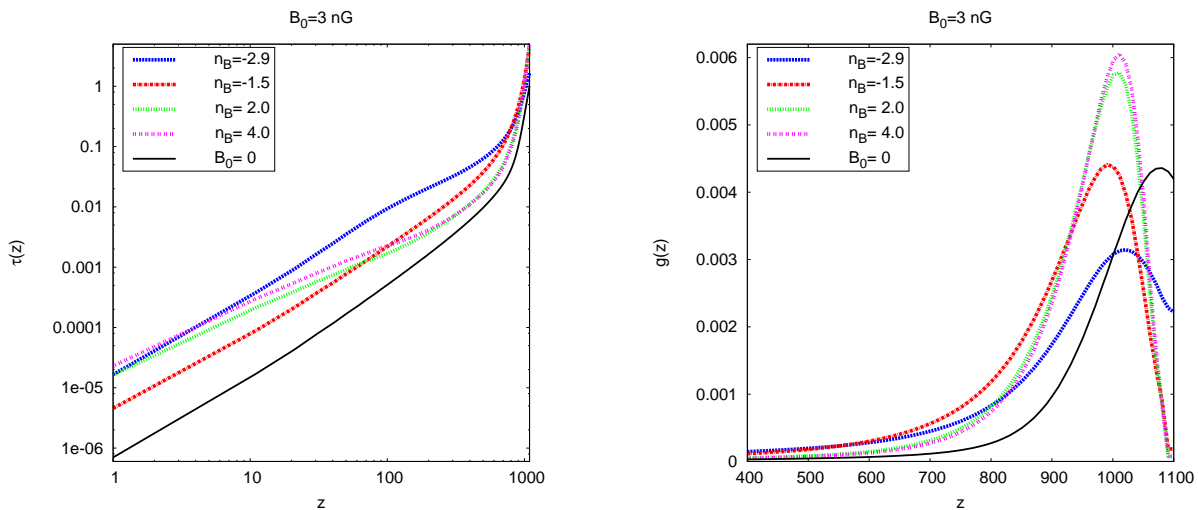


Figure 14. Optical depth to Thomson scattering from the present epoch to a given redshift, $\tau(z)$ (left panel), and the corresponding visibility function, $g(z)$ (right panel). A present-day magnetic field of $B_0 = 3$ nG, smoothed over $k_{d,dec}$ (Eq. (2.4) with $\cos\theta = 1$), is assumed. Ambipolar diffusion and decaying MHD turbulence are included. We explore four different values of the spectral index ($n_B = -2.9, -1.5, 2$, and 4). The black solid lines show the case of no magnetic field.

We find that the COBE/FIRAS bound on y is satisfied for $B_0 < 5$ nG for all values of n_B . The expected PIXIE bound, $y < 10^{-8}$, would exclude $B_0 > 1.0$ and 0.6 nG for $n_B = -2.9$ and -2.3 , respectively. As the predicted magnitude of y is insensitive to bluer spectral indices, we find that the expected PIXIE bound on y would exclude $B_0 > 0.6$ nG for all values of $n_B \geq 2$.

3.4 Optical depth to Thomson scattering

As shown in figure 10, heating due to dissipation of fields induces collisional ionization of the IGM. The optical depth to Thomson scattering resulting from this ionization, integrated from the present epoch to a given redshift z , is given by

$$\tau(z)_{B_0, n_B} = \int_0^z dz' \frac{\sigma_{TC}}{H(z')(1+z')} n_{e, B_0, n_B}(z'). \quad (3.9)$$

The left panel of figure 14 shows $\tau(z)_{B_0, n_B}$ for $B_0 = 3$ nG, while the right panel shows the visibility function defined by $g(z) \equiv \frac{dT}{dz} e^{-\tau(z)}$. Strikingly, even a few nG field yields the optical depth to $z \sim 10^3$ of order unity, which is clearly ruled out by the fact that we can still see the CMB temperature power spectrum at $l \gtrsim 100$. Therefore, the optical depth provides an additional constraint on the field strength [26].

How much optical depth is allowed by the current CMB data? The large-scale polarization of CMB at $l \lesssim 10$ constrains the optical depth up to $z \sim 20$ (see, e.g., ref. [58]), while the CMB temperature power spectrum at $l \gtrsim 100$ constrains the optical depth all the way up to the decoupling epoch. As almost all of the optical depth from collisional ionization due to dissipation of fields is generated at $z \sim 10^3$, the constraint from the temperature power spectrum is most relevant. However, the optical depth determined from the temperature power spectrum is correlated with the amplitude and tilt of primordial fluctuations.

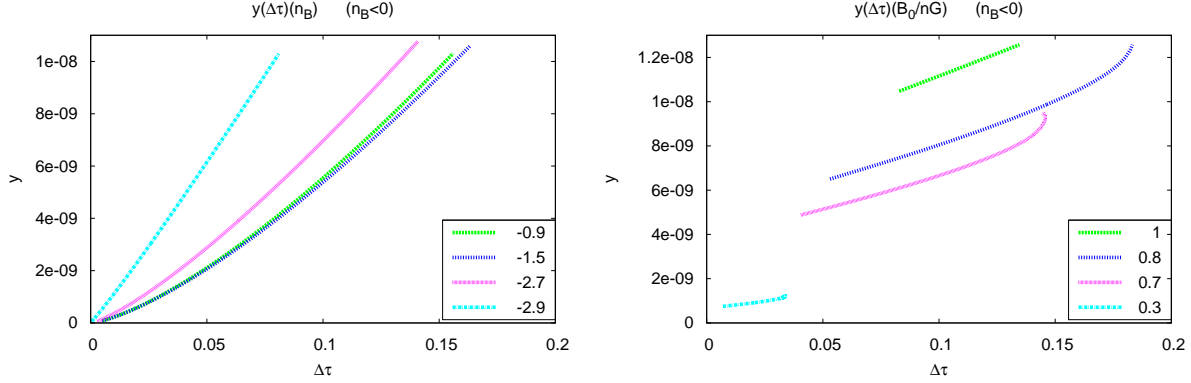


Figure 15. Correlations between y and $\Delta\tau$ for $n_B < 0$. (Left panel) The correlations shown for $n_B = -2.9, -2.7, -1.5,$ and -0.9 . (The field values, B_0 , vary along each line.) (Right panel) The correlations shown for $B_0 = 0.3, 0.7, 0.8,$ and 1 nG. (The spectral indices, n_B , vary along each line.)

The recently-released *Planck* data are able to break this correlation between parameters, yielding $\tau = 0.089 \pm 0.032$ (68% CL) *without using the polarization data* [59]. On the other hand, *WMAP*'s polarization data on large angular scales constrain the optical depth from reionization of the universe at $z \lesssim 20$ as $\tau = 0.089 \pm 0.014$ [27]. Taking the $2\text{-}\sigma$ limits, the total optical depth may be as high as $\tau_{\text{tot}} = 0.15$, while the reionization optical depth may be as low as $\tau_{\text{reion}} = 0.061$. Therefore, one may still “hide” the optical depth of $\Delta\tau \sim 0.1$ from a higher-redshift universe.⁷

We calculate the additional contribution to the optical depth due to the presence of a large-scale magnetic field between the decoupling and present epochs as

$$\Delta\tau(B_0, n_B) \equiv \tau_{B_0, n_B}(z_{\text{dec}}) - \tau_{B_0=0}(z_{\text{dec}}). \quad (3.10)$$

For $z_{\text{dec}} = 1088$, we find convenient numerical fits to our results:

$$\Delta\tau(B_0, n_B) = \begin{cases} 0.3(-n_B)^{0.08} \left(\frac{B_0}{\text{nG}}\right)^{1.72} \\ -0.03(-n_B)^{0.75} \left(\frac{B_0}{\text{nG}}\right)^{1.63} e^{1.8 \times 10^{-3}(-n_B)^{6.18}}, & n_B < 0 \\ 0.27n_B^{-0.02} \left(\frac{B_0}{\text{nG}}\right)^{1.78}, & n_B > 0. \end{cases} \quad (3.11)$$

We also find numerical fits for the y -type distortion:

$$y(B_0, n_B) = \begin{cases} 2.30 \times 10^{-8}(-n_B)^{7.8 \times 10^{-3}} \left(\frac{B_0}{\text{nG}}\right)^{2.42} \\ -1.04 \times 10^{-9}(-n_B)^{1.62} \left(\frac{B_0}{\text{nG}}\right)^{2.67} e^{1.07 \times 10^{-3}(-n_B)^{6.19}}, & n_B < 0 \\ 2.18 \times 10^{-8}n_B^{0.04} \left(\frac{B_0}{\text{nG}}\right)^{2.49}, & n_B > 0. \end{cases} \quad (3.12)$$

⁷However, more thorough analysis is required if we wish to find precisely how much optical depth is allowed in a higher-redshift universe, as dissipation of fields shifts the peak of the visibility function to $z \sim 1000$ from $z = 1088$ (see the right panel of figure 14), delaying the epoch of decoupling. This can modify the CMB temperature power spectrum significantly.

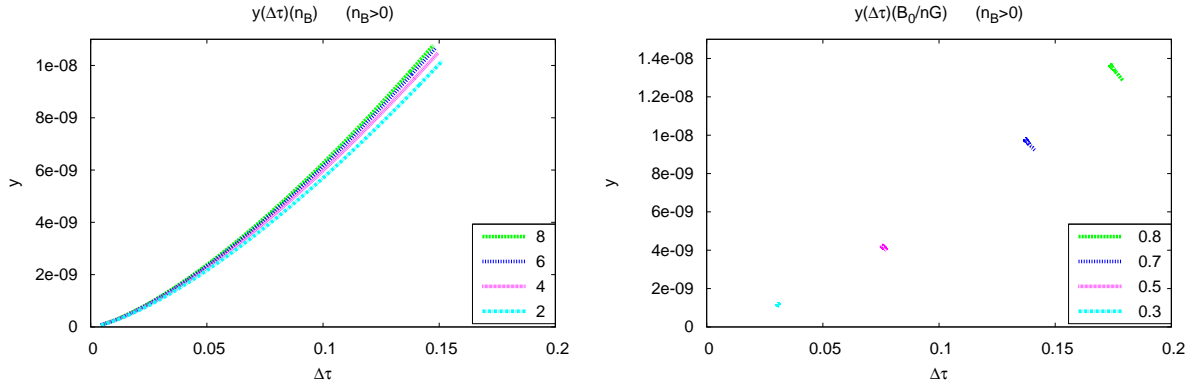


Figure 16. Correlations between y and $\Delta\tau$ for $n_B \geq 20$. (Left panel) The correlations shown for $n_B = 2, 4, 6,$ and 8 . (The field values, B_0 , vary along each line.) (Right panel) The correlations shown for $B_0 = 0.3, 0.5, 0.7,$ and 0.8 nG. (The spectral indices, n_B , vary along each line.)

As both $\Delta\tau$ and y are unique functions of n_B and B_0 , there is a tight correlation between $\Delta\tau$ and y . We show the correlations for $n_B < 0$ and $n_B \geq 2$ in figures 15 and 16, respectively. We find that $\Delta\tau \lesssim 0.1$ restricts the predicted y -type distortion to $y \lesssim 10^{-8}$ (with the precise values depending on n_B).

4 Conclusions

Dissipation of the energy in magnetic fields into the plasma in the pre-decoupling era as well as that into the IGM in the post-decoupling era heats photons of the CMB, creating both y - and μ -type distortions of the black-body spectrum of the CMB [25, 26].

In the pre-decoupling era, fast magnetosonic waves damp at the photon diffusion scale, k_γ , whereas slow magnetosonic waves and Alfvén waves damp at significantly a larger wavenumber, $k_\gamma/v_A \gg k_\gamma$ [23, 24]. As a result, if the total energy is divided equally between fast and slow magnetosonic waves and Alfvén waves, dissipation of the energy in the fields is dominated by that of slow magnetosonic waves and Alfvén waves. Dissipation during the “ μ -era,” $5 \times 10^4 \lesssim z \lesssim 2 \times 10^6$, creates a μ -type distortion, and that after the μ -era creates a y -type distortion.

We find that the y - and μ -type distortions from the pre-decoupling era provide the same limits on the field strength for a scale-invariant power spectrum of the fields. However, the μ -type distortion provides stronger limits for non-scale-invariant spectra, $n_B \gtrsim -2.9$, as a larger amount of energy is dissipated at higher redshifts for these spectra.

In the post-decoupling era, the MHD turbulence develops as radiative viscosity becomes negligible. Non-linear effects then lead to a decay of the MHD turbulence, leading to dissipation of the magnetic energy. Also, a separation of charged and neutral particles in the IGM by the Lorentz force induces a velocity difference between ionized and neutral components. The magnetic energy is then dissipated via ambipolar diffusion, as the velocity difference is damped by ion-neutral collisions. Both of these effects significantly alter the thermal and ionization history of the IGM in the post-decoupling era [26], creating a y -type distortion.

We find that decaying MHD turbulence and ambipolar diffusion dominate at different epochs, with the former dominating at higher redshifts, e.g., $z \gtrsim 100$ for $n_B = -1.5$. They have the opposite dependence on n_B : the larger the n_B is, the larger the effect of ambipolar diffusion becomes, and the smaller the effect of decaying MHD turbulence becomes. This makes the predicted temperature of the IGM relatively robust. For the present-day field strength of $B_0 = 3$ nG smoothed over $k_{d,dec}$ given by eq. (2.4) with $\cos\theta = 1$, we find that the IGM temperature can rise to ≈ 1000 to 2600 K at $z \gtrsim 10$ for all values of $-2.9 \leq n_B \leq 4$. (However, the temperature does not increase much beyond this for larger field values, as electrons cool via inverse Compton scattering off the CMB photons.) Such a high temperature modifies the ionization state of the IGM via collisional ionization, yielding the ionization fraction of order 10^{-3} at $z \gtrsim 10$.

The most significant finding in this paper is that a few nG field smoothed over $k_{d,dec}$ can easily produce $y \approx 10^{-7}$ in the post-decoupling era. While $y \approx 10^{-7}$ is small, it is well within sensitivity of the current technology, and a proposed experiment such as PIXIE would detect $y \approx 10^{-7}$ at the $50\text{-}\sigma$ level [41]. Therefore, such an experiment will be a powerful probe of the existence of intergalactic (possibly primordial) magnetic fields.

On the other hand, early ionization of the IGM due to dissipation of fields can provide a substantial contribution to the optical depth to Thomson scattering [26]. Requiring the additional contribution not to exceed $\Delta\tau \sim 0.1$ (which seems compatible with the current limits from the CMB temperature and polarization power spectra), we find that the predicted y -type distortion is restricted to $y \lesssim 10^{-8}$.

A challenge would be to distinguish the y -type distortion due to dissipation of fields from the other known contributions from virialized halos in $z \lesssim 5$ via the thermal Sunyaev-Zel'dovich effect, $y_{tSZ} \approx 1.7 \times 10^{-6}$ [57], and the reionization of the universe at $5 \lesssim z \lesssim 10$, $y_{reion} \approx 1.5 \times 10^{-7}$. The thermal Sunyaev-Zel'dovich effect is correlated with the large-scale structure of the universe traced by galaxies and galaxy clusters, whereas the reionization signal is correlated with 21-cm lines from neutral hydrogen during the reionization epoch. These correlations may be used to distinguish between the sources of the post-decoupling y -type distortion.

5 Acknowledgements

We would like to thank Jens Chluba and Rishi Khatri for useful discussion. KEK would like to thank the Max-Planck-Institute for Astrophysics for hospitality where this work was initiated. KEK acknowledges financial support by Spanish Science Ministry grants FIS2012-30926 and CSD2007-00042. We acknowledge the use of the Legacy Archive for Microwave Background Data Analysis (LAMBDA). Support for LAMBDA is provided by the NASA Office of Space Science.

A Photon diffusion scale

Including polarization, the photon diffusion scale is given by [15]

$$k_\gamma^{-2}(z) = \int_z^\infty \frac{dz}{6H(z)(1+R)\dot{\tau}} \left(\frac{16}{15} + \frac{R^2}{1+R} \right). \quad (\text{A.1})$$

The baryon-to-photon density ratio, R , is given by $R = \frac{3}{4} \frac{\Omega_{b,0}}{\Omega_{\gamma,0}} (1+z)^{-1}$. For the best-fit parameters of the WMAP 9-year data only ($\Omega_{b,0}h^2 = 0.02264$ and $\Omega_{\gamma,0}h^2 = 2.471 \times 10^{-5} \left(\frac{T}{2.725\text{K}} \right)^4$)

[40]), the numerical pre-factor evaluates to 687.171. Since $z > 1000$, it is a good approximation to neglect R . For the expansion rate, we use $H(z) = H_0 \Omega_{r,0}^{\frac{1}{2}} (1+z)^2 \left(1 + \frac{1+z_{eq}}{1+z}\right)^{\frac{1}{2}}$ where $\Omega_{r,0} = 1.69 \Omega_{\gamma,0}$ is the present-day total density of relativistic species including the standard value for the effective number of light neutrinos, $N_\nu = 3.04$. The epoch of radiation-matter equality is given by $\Omega_{r,0} = \Omega_{m,0}/(1+z_{eq})$. Thus

$$k_\gamma^{-2} \simeq \frac{8}{45} H_0^{-1} \Omega_{r,0}^{-\frac{1}{2}} \int_z^\infty \frac{dz}{z^2 \left(1 + \frac{z_{eq}}{z}\right)^{\frac{1}{2}} \dot{\tau}}. \quad (\text{A.2})$$

Following [28] the differential optical depth can be approximated by

$$\dot{\tau}(z) = \frac{c_2}{1000} \Omega_b^{c_1} \left(\frac{z}{1000}\right)^{c_2-1} \frac{\dot{a}}{a} (1+z), \quad (\text{A.3})$$

where a dot indicates the derivatives w.r.t. conformal time, $c_1 = 0.43$, and $c_2 = 16 + 1.8 \ln \Omega_b$. We compute the ionization fraction using $x_e(z) = \min(\dot{\tau}(n_e \sigma_T \frac{a}{a_0})^{-1}, 1)$, where

$$\left(n_e(z) \sigma_T \frac{a}{a_0}\right)^{-1} = 4.34 \times 10^4 \left(1 - \frac{Y_p}{2}\right)^{-1} (\Omega_b h^2)^{-1} \left(\frac{T}{2.725\text{K}}\right)^{-3} (1+z)^{-2} \text{ Mpc}. \quad (\text{A.4})$$

For the best-fit parameters of the *WMAP* 9-year data only, x_e calculated using the expression (A.3) is larger than one for $z > z_* \simeq 1486.57$. Thus, the differential optical depth is given by eq. (A.3) for $z_{\text{dec}} < z < z_*$ and by $\dot{\tau} = n_e \sigma_T \frac{a}{a_0}$ for $z \geq z_*$.

Deep inside the radiation-dominated era, the photon diffusion scale approaches

$$k_\gamma^{-2} \rightarrow A_\gamma^2 z^{-3}, \quad (\text{A.5})$$

where $A_\gamma^2 = 5.9807 \times 10^{10} \text{ Mpc}^2$ for the best-fit parameters of the *WMAP* 9-year data only. This is compared with the exact numerical result in the right panel of figure 17.

For completeness we give the expressions for k_γ^{-2} in $z \geq z_*$,

$$\begin{aligned} k_{\gamma, z \geq z_*}^{-2}(z) &= 2.16567 \times 10^7 (\Omega_{r,0} h^2)^{-\frac{1}{2}} \left(1 - \frac{Y_p}{2}\right)^{-1} (\Omega_b h^2)^{-1} \\ &\times \int_z^\infty dz (1+z)^{-\frac{7}{2}} (2+z+z_{eq})^{-\frac{1}{2}} (1+R)^{-1} \left(\frac{16}{15} + \frac{R^2}{1+R}\right) \text{ Mpc}^2 \end{aligned} \quad (\text{A.6})$$

and in $z_{\text{dec}} < z < z_*$,

$$\begin{aligned} k_{\gamma, z < z_*}^{-2}(z) &= 1.49402 \times 10^6 (\Omega_{r,0} h^2)^{-1} \Omega_b^{-c_1} c_2^{-1} 10^{3c_2} \\ &\times \int_z^{z_*} dz (1+z)^{-3} (2+z+z_{eq})^{-1} z^{1-c_2} (1+R)^{-1} \left(\frac{16}{15} + \frac{R^2}{1+R}\right) \text{ Mpc}^2 \\ &+ k_{\gamma, z \geq z_*}^{-2}(z_*). \end{aligned} \quad (\text{A.7})$$

The evolution of k_γ^{-1} is shown in the left panel of figure 17, which clearly shows the significant increase in the photon mean free path close to decoupling.

For the parameters of the *WMAP* 9-year data only, the maximal damping wave number at decoupling computed from eq. (A.7) is

$$k_{d,dec} = 286.91 \left(\frac{B_0}{\text{nG}}\right)^{-1} \text{ Mpc}^{-1}. \quad (\text{A.8})$$

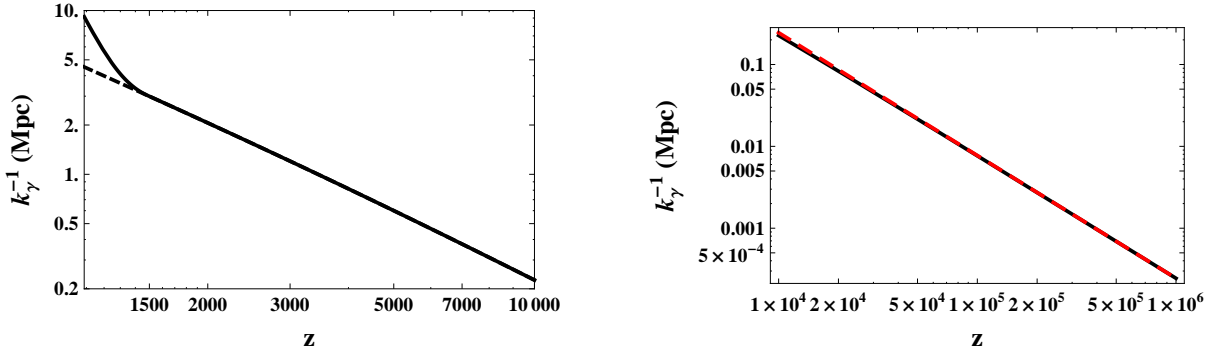


Figure 17. Photon diffusion scale as a function of z . (Left panel) For $z < 10^4$. The solid line shows the results using eqs. (A.6) and (A.7). The dashed line shows the photon diffusion scale for instantaneous recombination. (Right panel) For $z > 10^4$. The solid (black) line shows the results using eq. (A.6), while the dashed (red) line shows the approximation in the radiation-dominated era, eq. (A.5).

References

- [1] J. C. Mather, E. Cheng, R. Shafer, C. Bennett, N. Boggess, et al., *A Preliminary measurement of the Cosmic Microwave Background spectrum by the Cosmic Background Explorer (COBE) satellite*, *Astrophys.J.* **354** (1990) L37–L40.
- [2] J. C. Mather, E. Cheng, D. Cottingham, R. Eplee, D. Fixsen, et al., *Measurement of the Cosmic Microwave Background spectrum by the COBE FIRAS instrument*, *Astrophys.J.* **420** (1994) 439–444.
- [3] D. Fixsen, E. Cheng, J. Gales, J. C. Mather, R. Shafer, et al., *The Cosmic Microwave Background spectrum from the full COBE FIRAS data set*, *Astrophys.J.* **473** (1996) 576, [[astro-ph/9605054](#)].
- [4] A. F. Illarionov and R. A. Sunyaev, *Comptonization, characteristic radiation spectra, and thermal balance of low-density plasma*, *Soviet Astronomy* **18** (1975) 413–419.
- [5] A. F. Illarionov and R. A. Sunyaev, *Comptonization, the background-radiation spectrum, and the thermal history of the universe*, *Soviet Astronomy* **18** (1975) 691–699.
- [6] L. Danese and G. de Zotti, *Double Compton process and the spectrum of the microwave background*, *Astron.Astrophys.* **107** (1982) 39–42.
- [7] C. Burigana, L. Danese, and G. de Zotti, *Formation and evolution of early distortions of the microwave background spectrum - A numerical study*, *Astron.Astrophys.* **246** (1991) 49–58.
- [8] R. Weymann, *The Energy Spectrum of Radiation in the Expanding Universe*, *Astrophys.J.Lett.* **145** (1966) 560.
- [9] Y. B. Zel’dovich and R. A. Sunyaev, *The Interaction of Matter and Radiation in a Hot-Model Universe*, *Astrophys.Space Sci.* **4** (1969) 301.
- [10] R. Sunyaev and Y. Zel’dovich, *The Interaction of matter and radiation in the hot model of the universe*, *Astrophys.Space Sci.* **7** (1970) 20–30.
- [11] J. Chluba and R. A. Sunyaev, *The evolution of CMB spectral distortions in the early Universe*, *Mon.Not.Roy.Astron.Soc.* **419** (2012) 1294–1314, [[arXiv:1109.6552](#)].
- [12] R. Khatri and R. A. Sunyaev, *Beyond y and μ : the shape of the CMB spectral distortions in the intermediate epoch, $.5 \times 10^4 \lesssim z \lesssim 2 \times 10^5$* , *JCAP* **9** (2012) 16, [[arXiv:1207.6654](#)].

- [13] J. Silk, *Cosmic black body radiation and galaxy formation*, *Astrophys.J.* **151** (1968) 459–471.
- [14] P. Peebles and J. Yu, *Primeval adiabatic perturbation in an expanding universe*, *Astrophys.J.* **162** (1970) 815–836.
- [15] N. Kaiser, *Small-angle anisotropy of the microwave background radiation in the adiabatic theory*, *Mon.Not.Roy.Astron.Soc.* **202** (1983) 1169–1180.
- [16] R. A. Sunyaev and Y. B. Zel’dovich, *The interaction of matter and radiation in the hot model of the Universe, II*, *Astrophys.Space Sci.* **7** (1970) 20–30.
- [17] R. A. Sunyaev and Y. B. Zel’dovich, *Small scale entropy and adiabatic density perturbations – Antimatter in the Universe*, *Astrophys.Space Sci.* **9** (1970) 368–382.
- [18] R. A. Daly, *Spectral distortions of the microwave background radiation resulting from the damping of pressure waves*, *Astrophys.J.* **371** (1991) 14–28.
- [19] Y. B. Zel’dovich, A. F. Illarionov, and R. A. Sunyaev, *The Effect of Energy Release on the Emission Spectrum in a Hot Universe*, *Soviet Journal of Experimental and Theoretical Physics* **35** (1972) 643.
- [20] R. Khatri, R. A. Sunyaev, and J. Chluba, *Mixing of blackbodies: entropy production and dissipation of sound waves in the early Universe*, *Astron.Astrophys.* **543** (2012) A136, [[arXiv:1205.2871](#)].
- [21] J. Chluba, R. Khatri, and R. A. Sunyaev, *CMB at 2×2 order: the dissipation of primordial acoustic waves and the observable part of the associated energy release*, *Mon.Not.Roy.Astron.Soc.* **425** (2012) 1129–1169, [[arXiv:1202.0057](#)].
- [22] E. Pajer and M. Zaldarriaga, *A hydrodynamical approach to CMB μ -distortion from primordial perturbations*, *JCAP* **1302** (2013) 036, [[arXiv:1206.4479](#)].
- [23] K. Jedamzik, V. Katalinic, and A. V. Olinto, *Damping of cosmic magnetic fields*, *Phys.Rev.* **D57** (1998) 3264–3284, [[astro-ph/9606080](#)].
- [24] K. Subramanian and J. D. Barrow, *Magnetohydrodynamics in the early universe and the damping of nonlinear Alfvén waves*, *Phys.Rev.* **D58** (1998) 083502, [[astro-ph/9712083](#)].
- [25] K. Jedamzik, V. Katalinic, and A. V. Olinto, *A Limit on primordial small scale magnetic fields from CMB distortions*, *Phys.Rev.Lett.* **85** (2000) 700–703, [[astro-ph/9911100](#)].
- [26] S. K. Sethi and K. Subramanian, *Primordial magnetic fields in the post-recombination era and early reionization*, *Mon.Not.Roy.Astron.Soc.* **356** (2005) 778–788, [[astro-ph/0405413](#)].
- [27] **WMAP** Collaboration, G. Hinshaw et al., *Nine-Year Wilkinson Microwave Anisotropy Probe (WMAP) Observations: Cosmological Parameter Results*, *Astrophys.J.Suppl.* **208** (2013) 19, [[arXiv:1212.5226](#)].
- [28] W. Hu and N. Sugiyama, *Anisotropies in the cosmic microwave background: An Analytic approach*, *Astrophys.J.* **444** (1995) 489–506, [[astro-ph/9407093](#)].
- [29] M. S. Turner and L. M. Widrow, *Inflation Produced, Large Scale Magnetic Fields*, *Phys.Rev.* **D37** (1988) 2743.
- [30] T. Vachaspati, *Magnetic fields from cosmological phase transitions*, *Phys.Lett.* **B265** (1991) 258–261.
- [31] M. Joyce and M. E. Shaposhnikov, *Primordial magnetic fields, right-handed electrons, and the Abelian anomaly*, *Phys.Rev.Lett.* **79** (1997) 1193–1196, [[astro-ph/9703005](#)].
- [32] J. Ahonen and K. Enqvist, *Magnetic field generation in first order phase transition bubble collisions*, *Phys.Rev.* **D57** (1998) 664–673, [[hep-ph/9704334](#)].
- [33] D. Grasso and H. R. Rubinstein, *Magnetic fields in the early universe*, *Phys.Rept.* **348** (2001) 163–266, [[astro-ph/0009061](#)].

- [34] L. M. Widrow, *Origin of galactic and extragalactic magnetic fields*, *Rev.Mod.Phys.* **74** (2002) 775–823, [[astro-ph/0207240](#)].
- [35] M. Giovannini, *The Magnetized universe*, *Int.J.Mod.Phys.* **D13** (2004) 391–502, [[astro-ph/0312614](#)].
- [36] A. Kandus, K. E. Kunze, and C. G. Tsagas, *Primordial magnetogenesis*, *Phys.Rept.* **505** (2011) 1–58, [[arXiv:1007.3891](#)].
- [37] R. Durrer and C. Caprini, *Primordial magnetic fields and causality*, *JCAP* **0311** (2003) 010, [[astro-ph/0305059](#)].
- [38] R. Khatri, R. A. Sunyaev, and J. Chluba, *Does Bose-Einstein condensation of CMB photons cancel μ distortions created by dissipation of sound waves in the early Universe?*, *Astron.Astrophys.* **540** (2012) A124, [[arXiv:1110.0475](#)].
- [39] W. Hu and J. Silk, *Thermalization and spectral distortions of the cosmic background radiation*, *Phys.Rev.* **D48** (1993) 485–502.
- [40] **Particle Data Group** Collaboration, J. Beringer et al., *Review of Particle Physics (RPP)*, *Phys.Rev.* **D86** (2012) 010001.
- [41] A. Kogut, D. Fixsen, D. Chuss, J. Dotson, E. Dwek, et al., *The Primordial Inflation Explorer (PIXIE): A Nulling Polarimeter for Cosmic Microwave Background Observations*, *JCAP* **1107** (2011) 025, [[arXiv:1105.2044](#)].
- [42] D. R. Schleicher, R. Banerjee, and R. S. Klessen, *Reionization - A probe for the stellar population and the physics of the early universe*, *Phys.Rev.* **D78** (2008) 083005, [[arXiv:0807.3802](#)].
- [43] K. E. Kunze, *CMB anisotropies in the presence of a stochastic magnetic field*, *Phys.Rev.* **D83** (2011) 023006, [[arXiv:1007.3163](#)].
- [44] D. R. Schleicher, R. Banerjee, and R. S. Klessen, *Influence of primordial magnetic fields on 21 cm emission*, *Astrophys.J.* **692** (2009) 236–245, [[arXiv:0808.1461](#)].
- [45] M. Christensson, M. Hindmarsh, and A. Brandenburg, *Inverse cascade in decaying 3-D magnetohydrodynamic turbulence*, *Phys.Rev.* **E64** (2001) 056405, [[astro-ph/0011321](#)].
- [46] R. Banerjee and K. Jedamzik, *The Evolution of cosmic magnetic fields: From the very early universe, to recombination, to the present*, *Phys.Rev.* **D70** (2004) 123003, [[astro-ph/0410032](#)].
- [47] S. Seager, D. D. Sasselov, and D. Scott, *A new calculation of the recombination epoch*, *Astrophys.J.* **523** (1999) L1–L5, [[astro-ph/9909275](#)].
- [48] S. Seager, D. D. Sasselov, and D. Scott, *How exactly did the universe become neutral?*, *Astrophys.J.Suppl.* **128** (2000) 407–430, [[astro-ph/9912182](#)].
- [49] W. Y. Wong, A. Moss, and D. Scott, *How well do we understand cosmological recombination?*, *Mon.Not.Roy.Astron.Soc.* (2007) [[arXiv:0711.1357](#)].
- [50] J. Chluba and R. M. Thomas, *Towards a complete treatment of the cosmological recombination problem*, *Mon.Not.Roy.Astron.Soc.* **412** (2011) 748–764, [[arXiv:1010.3631](#)].
- [51] J. A. Rubiño-Martín, J. Chluba, W. A. Fendt, and B. D. Wandelt, *Estimating the impact of recombination uncertainties on the cosmological parameter constraints from cosmic microwave background experiments*, *Mon.Not.Roy.Astron.Soc.* **403** (2010) 439–452, [[arXiv:0910.4383](#)].
- [52] J. Chluba, *Could the cosmological recombination spectrum help us understand annihilating dark matter?*, *Mon.Not.Roy.Astron.Soc.* **402** (2010) 1195–1207, [[arXiv:0910.3663](#)].
- [53] J. Chluba, G. M. Vasil, and L. J. Dursi, *Recombinations to the Rydberg states of hydrogen and their effect during the cosmological recombination epoch*, *Mon.Not.Roy.Astron.Soc.* **407** (2010) 599–612, [[arXiv:1003.4928](#)].

- [54] E. R. Switzer and C. M. Hirata, *Primordial helium recombination. 3. Thomson scattering, isotope shifts, and cumulative results*, *Phys.Rev.* **D77** (2008) 083008, [[astro-ph/0702145](#)].
- [55] D. Grin and C. M. Hirata, *Cosmological hydrogen recombination: The effect of extremely high- n states*, *Phys.Rev.* **D81** (2010) 083005, [[arXiv:0911.1359](#)].
- [56] Y. Ali-Haïmoud and C. M. Hirata, *Ultrafast effective multi-level atom method for primordial hydrogen recombination*, *Phys.Rev.* **D82** (2010) 063521, [[arXiv:1006.1355](#)].
- [57] A. Refregier, E. Komatsu, D. N. Spergel, and U.-L. Pen, *Power spectrum of the Sunyaev-Zel'dovich effect*, *Phys.Rev.* **D61** (2000) 123001, [[astro-ph/9912180](#)].
- [58] M. Zaldarriaga, L. Colombo, E. Komatsu, A. Lidz, M. Mortonson, et al., *CMBPol Mission Concept Study: Reionization Science with the Cosmic Microwave Background*, [arXiv:0811.3918](#).
- [59] **Planck Collaboration** Collaboration, P. Ade et al., *Planck 2013 results. XVI. Cosmological parameters*, *ArXiv e-prints* (2013) [[arXiv:1303.5076](#)].